LAWRENCE
LIVERMORE
NATIONAL
LABORATORY

UCRL-JRNL-219094

Wideband Multichannel Time-Reversal Processing for Acoustic Communications in a Tunnel-like Structure

J. V. Candy, D. H. Chambers, C. L. Robbins, B. L. Guidry, A. J. Poggio, F. Dowla, C. A. Hertzog

February 17, 2006

Journal of the Acoustical Society of America

Wideband multichannel time-reversal processing for acoustic communications in a tunnel-like structure

James V. Candy[♦], David H. Chambers, Christopher L. Robbins, Brian L. Guidry, Andrew J. Poggio, Farid Dowla, Claudia A. Hertzog

University of California, Lawrence Livermore National Laboratory
P.O. Box 808, Livermore, CA 94551

Received.

The development of multichannel time-reversal (T/R) processing techniques continues to progress rapidly especially when the need to communicate in a highly reverberative environment becomes critical. The underlying T/R concept is based on time-reversing the Green's function characterizing the uncertain communications channel investigating the deleterious dispersion and multipath effects. In this paper, attention is focused on two major objectives: (1) wideband communications leading to a time reference modulation technique; and (2) multichannel acoustic communications in a tunnel (or cave or pipe) with many obstructions, multipath returns, severe background noise, disturbances, long propagation paths (~180') with disruptions (bends). For this extremely hostile environment, it is shown that multichannel T/R receivers can easily be extended to the wideband designs while demonstrating their performance in both the "canonical" stairwell of our previous work as well as a tunnel-like structure. Acoustic information signals are transmitted with an 8-element host or base station array to two client receivers with a significant loss in signal levels due to the propagation environment. In this paper, the results of the new wideband T/R processor and modulation scheme are discussed to demonstrate the overall performance for both high (24-bit) and low (1-bit) bit level analog-to-digital (A/D) converter designs. These results are validated by performing proof-of-principle acoustic communications experiments in air. It is shown that the resulting T/R receivers are capable of extracting the transmitted coded sequence from noisy microphone array measurements with zero-bit error.

PACS numbers: 43.60.Dh, 43.28.We, 43.28.Tc

I. INTRODUCTION

Complex reverberant environments, especially enclosed tunnel-like structures, offer a distinct challenge to communications systems. Because of the enclosure, short reverberation paths evolve that can rapidly deteriorate the communications medium creating distortion and loss of signal levels due to destructive interference[1,2]. The need to communicate in such hostile environments prove important for a variety of applications based on military operations in caves and underground structures, a maze of buried pipes where systems attempt to communicate critical information about chemical anomalies jeopardizing a city or even the autonomous operations of independent robots servicing hazardous waste facilities in the future. In all of these cases, inherent obstructions cause transmitted signals to reflect, refract and disperse in a multitude of directions distorting both their shape and arrival times at network receiver locations. Thus this creates a problem in transmitting information in the form of waves throughout a complex

[♦] Currently on sabbatical leave at the University of Cambridge, Department of Engineering, Signal Processing Group, Trumpington Rd, Cambridge CB2 1PZ, U.K.

environment. Waves are susceptible to *multiple paths* and *distortions* created by a variety of possible obstructions present in tunnel-like environments. This is precisely the communications problem we solve using the physics of wave propagation to not only mitigate the noxious effects created by the hostile medium, but also to utilize it in a constructive manner enabling a huge benefit in communications. We use *time-reversal*[3,4] (T/R) pre-processing coupled with a wideband receiver design to accomplish this task.

Time-reversal is applied to reconstruct transmitted communication signals by *retracing* all of the multiple paths that originally distorted the transmitted signals. Contrary to intuitive notions, multipath propagation in a communications channel residing in a hostile environment can be considered a potential advantage by increasing the overall signal-to-noise ratio (SNR) --- when utilized properly. T/R communications is based on taking advantage of the multipath arrivals and multiple scatterers to enhance SNR. The basic communications problem is to transmit coded information through the hostile environment or medium and receive it at desired receiver or client stations. These client stations can also broadcast through the medium characterized by unique Green's function paths to create a two-way communication link as depicted in Fig. 1. Here we investigate the performance of wideband communication systems employing sensor arrays using multichannel processors for client stations in a hostile multipath/multiple scatterer environment.

The basic idea in wideband processing for communications is to transmit a narrow information pulse capable of carrying coded information while simultaneously interrogating the medium to extract a set of Green's functions for transmitter-receiver pairs. Many applications simply transmit a sharp, narrow pulse to approximate an impulse from the host thereby providing the Green's function response directly to the client receiver and then follow it with the coded information message[1,2]. This is the approach we take in this paper simultaneously estimating the channel response and transmitting coded information. We use a correlation-based receiver design coupled with T/R processing to extract the codes from noisy, reverberative data.

T/R communications evolved from the work of A. Parvulescu[5] where the underlying Green's function of the ocean was first estimated using a pilot signal or probe pulse, time reversed and retransmitted through the medium to focus and achieve a high SNR gain. The realization of multichannel T/R receivers is captured by a sequence of papers developing the theory[6,7]. Receiver realizations discussed in this case is equivalent to post-processing the received data with the estimated Green's functions, this work was followed by equivalent model-based methods[8,9]. Subsequent experiments to demonstrate the performance of T/R in the ocean channel followed[10-13]. Schemes related to that of this paper using a passive approach and correlation-based designs for incoherent communications in underwater acoustics[14-16] were recently developed. Exclusive T/R designs demonstrated the effectiveness of a variety of T/R receiver realizations in a highly reverberant environment for point-to-point and array-to-point communications[17,18]. The work we present in this paper extends these results to the wideband case for both multi-bit resolution (24-bit analog-to-digital (A/D) conversion) and the minimal resolution "1-bit" T/R receiver designs[18]. The realizations of various 1-bit T/R receivers

are discussed and applied to noisy microphone array measurements in a hostile environment tunnel-like environment.

In Sec. II, the underlying T/R theory relative to the multichannel communication problem is briefly discussed including the development of the wideband time-reference (*TRef*) receivers and other essential components of an acoustics communications system. We also include the corresponding 1-bit realization for compare them with the narrowband designs in the well-known stairwell environment[17,18]. The development of a suite of experiments to assess the feasibility and performance of the T/R receivers is described in Sec. III along with the associated signal processing. Finally, we summarize these results and discuss future efforts.

II. T/R COMMUNICATIONS: A BRIEF REVIEW

In this section we briefly discuss the suite of "wideband" multichannel time-reversal receivers used to recover a transmitted information sequence or code from a set of receiver measurements in a reverberant, temporally stationary environments. The emphasis is on the processing provided by the various realizations to extract the information signal and characterize receiver performance. Subsequent experiments are performed to demonstrate the feasibility of using wideband time-reversal designs to extract the coded information sequence.

A. Time-Reversal Background

The detection of a transmitted information sequence can be transformed to the problem of maximizing the output signal-to-noise ratio, SNR_{out}, at the receiver of a communications system. This problem is termed the matched-filter problem and is: *given* a "known" signal, $s(t)$, in additive white noise, *find* the filter response, $f(t)$, that maximizes the SNR_{out}. Its solution is classical and reduces to applying the Schwartz inequality[1,2] yielding the optimal solution, $f(t) = s(T-t)$, the reversed, shifted signal or replicant. The matched-filtering operation, $mf(t)$, is then simply the cross-correlation function of the known signal, $s(t)$, with the measurement, $z(r;t)$, that is, $C_{sz}(T-t)$.

The matched-filter problem for time-reversal is identical to the classical problem with a "known" Green's function of the medium replacing the known replicant.[3,4] The Green's function, $g(r,r_o;t)$, is the result of a point-to-point communications link between a *host* station or base station (source) at r_o to a *client* (receiver) at r. In the T/R case, the matched-filter solution is again found by maximizing the output SNR leading to $f(t) = g(r,r_o;T-t)$. Thus, for T/R, the optimal matched-filter solution is the time-reversed Green's function from the host station-to-client station (source-to-receiver) or vice versa. Since T/R theory requires reciprocity[3,4], this result is valid for *both* transmission and reception, that is, $g(r,r_o;T-t) \leftrightarrow g(r_o,r;T-t)$. Note also that when an array is included to sample the spatial field or transmit a wave, then a solution evolves

with *sets* of Green's function transmitter-receiver pairs. These results include the focus at the client station (source) position, r_o, yielding the optimal, *spatio-temporal* matched-filter solution[3,4], $g(\mathbf{r}_\ell, \mathbf{r}_o; T-t)$ at sensor position, $\mathbf{r}_\ell$.

B. Multichannel T/R Receivers

In this section, we briefly review the multichannel communications problem from the signal processing perspective[17,18] and discuss the time-reversal solutions. In this paper our detailed results will primarily encompass receivers T/R I and III of Reference 18, therefore, we will limit this review to only those receivers. Note that the only major difference is to replace the estimated Green's function with the received pilot in both T/R II and IV designs.

Define the field received at the m^{th}-station spatially located at $\mathbf{r}_m$ and at time *t* by the spatio-temporal signal, $z(\mathbf{r}_m; t)$ and the excitation signal transmitted from the ℓ^{th} array element spatially located at $\mathbf{r}'_\ell$ and *t* by $x(\mathbf{r}'_\ell; t)$. The transmitted signal propagates through the time invariant medium characterized equivalently by its impulse response or Green's function, $g(\mathbf{r}_m, \mathbf{r}'_\ell; t)$, representing the propagation medium from the excitation signal (source array sensor) to the client receiver station. This *spatio-temporal propagation* relation can be written compactly as

$$\mathbf{z}(t) = \mathbf{G}(\mathbf{r}; t) * \mathbf{x}(t) \ , \tag{1}$$

where $\mathbf{z} \in \mathbf{C}^{M\times 1}$ is the received signal at all of the *M* stations, $\mathbf{x} \in \mathbf{C}^{L\times 1}$ is the information or message signal transmitted by the array into the medium represented by its transfer (impulse response) matrix, $\mathbf{G} \in \mathbf{C}^{M\times L}$ consisting of the channel impulse responses or equivalently Green's function, $g(\mathbf{r}_m, \mathbf{r}'_\ell; t)$, from the ℓ^{th}-transmit array sensor element to the m^{th}-receiver station. More compactly, if we define

$$g_{m\ell}(t) \equiv g(\mathbf{r}_m, \mathbf{r}'_\ell; t) \ , \tag{2}$$

then the propagation relation can be rewritten in the standard vector-matrix format where the indices identify the spatial path vector locations, that is, $(\mathbf{r}_m, \mathbf{r}'_\ell) \to (m, \ell)$ as depicted in Fig. 1. Here we define the *host* as the transmitting array and the *clients* as the receiving stations. The spatio-temporal propagation of Eq. (1) can now be expressed in terms of *L*-dimensional row vectors to give[♦]

[♦] Here vector-matrix operations hold with the convolution operator replacing the usual multiplication operator, that is, $\mathbf{x}^T(t) * \mathbf{y}(t) \equiv \left[x_1(t) \cdots x_N(t)\right] * \begin{bmatrix} y_1(t) \\ \vdots \\ y_N(t) \end{bmatrix} = \sum_{i=1}^{N} x_i(t) * y_i(t)$ [inner convolution].

$$\mathbf{z}(t) = \begin{bmatrix} \mathbf{g}_1^T(t) \\ \vdots \\ \mathbf{g}_M^T(t) \end{bmatrix} * \mathbf{x}(t) = \begin{bmatrix} \mathbf{g}_1^T(t) * \mathbf{x}(t) \\ \vdots \\ \mathbf{g}_M^T(t) * \mathbf{x}(t) \end{bmatrix}. \tag{3}$$

where the set of row vectors, $\mathbf{g}_m^T(t)$, define the propagation path of the transmitted signals from the array to the m^{th}-client station as in Fig. 1. At the m^{th}-client station the data received from the transmit array is therefore

$$z_m(t) = \mathbf{g}_m^T(t) * \mathbf{x}(t) = \sum_{\ell=1}^{L} g_{m\ell}(t) * x_\ell(t) \tag{4}$$

Note that we must first estimate the Green's function denoted by $\hat{g}(r;t)$ from measured pilot data in order to implement these designs. In signal processing this is called the system identification or equivalently parameter estimation problem and is readily solved using the well-known Wiener filter design techniques[19,20].

1. T/R RECEIVER I

The T/R I receiver realization is based on transmitting the time reversed, estimated Green's functions convolved on each array sensor channel with the information signal to the m^{th}-client receiver station. In this realization the transmitted code is given by

$$\mathbf{x}(t) = \hat{\mathbf{g}}_m(-t) \otimes i(t) = \begin{bmatrix} \hat{g}_{m1}(-t) * i(t) \\ \vdots \\ \hat{g}_{mL}(-t) * i(t) \end{bmatrix}, \tag{5}$$

where $\otimes$ is defined as the Kronecker convolution operator (element-by-element multiply) yielding a $L \times 1$ complex vector. Therefore from Eq. (1), we have that the wave propagated from the transmit array through the medium is

$$\mathbf{z}_{i\hat{g}_m X}(t) = \mathbf{G}(\mathbf{r};t) * \mathbf{x}(t) = \mathbf{G}(\mathbf{r};t) * \left(\hat{\mathbf{g}}_m(-t) \otimes i(t)\right), \tag{6}$$

with the subscript representing the information signal (i) convolved with the estimated Green's functions $(\hat{\mathbf{g}}_m)$ corresponding to the m^{th}-client station on transmission (X). This expression can be written as and shown to be[18]:

$$\mathbf{z}_{i\hat{g}_m X}(t) = \begin{bmatrix} \mathbf{g}_1^T(t) \\ \vdots \\ \mathbf{g}_M^T(t) \end{bmatrix} * \left(\hat{\mathbf{g}}_m(-t) \otimes i(t) \right) = \begin{bmatrix} \bar{C}_{g_1 \hat{g}_m}(t) \\ \vdots \\ \bar{C}_{g_M \hat{g}_m}(t) \end{bmatrix} \otimes i(t) \tag{7}$$

where the cross-correlations are defined by

$$\bar{C}_{g_k \hat{g}_m}(t) \equiv \sum_{\ell=1}^{L} C_{g_k \hat{g}_m}(\ell; t) \text{ for } C_{g_k \hat{g}_m}(\ell; t) \equiv g_{k\ell}(t) * \hat{g}_{m\ell}(-t) \text{ and } k = 1, \cdots, M \, .$$

Therefore at the k^{th}-client receiver station, we have

$$z_k(t) \equiv z_{i\hat{g}_m X}(k; t) = \bar{C}_{g_k \hat{g}_m}(t) * i(t) \, . \tag{8}$$

demonstrating that maximum coherence occurs when $k=m$, matching the set of Green's functions to the appropriate client receiver, since the auto rather than cross correlation is achieved demonstrating that the transmitted wavefield satisfies the time-reversal focusing principle[3,4]. The output of this realization, T/R I, at the receivers is simply, $\mathbf{R}_{i\hat{g}_m X}(t) = \mathbf{z}_{i\hat{g}_m X}(t)$ and over the entire communications network (M receiver stations) or at the k^{th}-client as (as before), $R_{i\hat{g}_m X}(k; t) = z_{i\hat{g}_m X}(k; t) = z_k(t)$.

2. T/R RECEIVER III

The realization for this receiver is also similar to that of T/R Receiver I; however, the reversed client receiver station set of Green's functions is performed on *reception* rather than transmission. Starting with the receiver input from the transmitted wavefield of Eq. 8 as

$$z_m(t) = \mathbf{g}_m^T(t) * \mathbf{i}(t) \, , \tag{9}$$

and convolving it with the estimated reversed Green's functions, we obtain

$$\mathbf{R}_{i\hat{g}_m R}(t) = z_m(t) * \hat{\mathbf{g}}_m(-t) = \left(\mathbf{g}_m^T(t) * \mathbf{i}(t) \right) * \hat{\mathbf{g}}_m(-t) = \left(\mathbf{g}_m^T(t) * \hat{\mathbf{g}}_m(-t) \right) * \mathbf{i}(t) \, , \tag{10}$$

where $\mathbf{R}_{i\hat{g}_m R}(t) \in \mathrm{R}^{L \times 1}$, $\mathbf{i}(t) = \mathbf{1} \cdot i(t)$ for $\mathbf{1} \in \mathrm{R}^{L \times 1}$, a vector of ones .

Intuitively, from the scalar case[6] results and T/R I, we expect that this vector signal should be summed over the sensor array to yield equivalent results, that is, T/R processing of this vector (array) data implies that each of the component vector outputs be summed, since they are aligned in phase from the basic nature of time-reversal. Therefore, this operation is equivalent to physically beam forming or focusing on receive[18]. Mathematically, re-arranging the receiver expression of Eq. (10) we have

$$\mathbf{R}_{i\hat{g}_m R}(t) = \hat{\mathbf{g}}_m(-t) * z_m(t) = \left(\hat{\mathbf{g}}_m(-t) * \mathbf{g}_m^T(t)\right) * = \mathbf{C}_\mathbf{m}(t) * \mathbf{i}(t), \tag{11}$$

for $\mathbf{C}_\mathbf{m}(t) \in \mathrm{R}^{L\times L}$, a *correlation matrix* with its cross-correlation components $C_{\hat{g}_k g_\ell}(m;t) \equiv \hat{g}_{mk}(-t) * g_{m\ell}(t)$ for $k = 1,\cdots,L; \ell = 1,\cdots,L$. This matrix can be interpreted physically, since the diagonals are the auto-correlations of the individual sensor elements focused (on reception) at the m^{th}-client receiver with the off-diagonals corresponding the sensor cross-correlations. Theoretically, T/R focusing conditions imply that the sensor cross-correlations terms should be null which is equivalent to the conditions that there is *no* mutual coupling between sensor elements. Thus, $\mathbf{C}_\mathbf{m}(t) \to \tilde{\mathbf{C}}_\mathbf{m}(t) \equiv \mathrm{diag}\left[\mathbf{C}_\mathbf{m}(t)\right]$.

The information vector is simply, $\mathbf{i}(t) = \mathbf{1}\cdot i(t)$ for $\mathbf{1} \in \mathrm{R}^{L\times 1}$, a vector of ones (as before). Therefore, assuming no mutual coupling, we have that cross-correlation terms vanish and

$$\mathbf{R}_{i\hat{g}_m R}(t) = \tilde{\mathbf{C}}_\mathbf{m}(t) * \mathbf{i}(t) = \begin{bmatrix} C_{\hat{g}_1 g_1}(m;t) \\ \vdots \\ C_{\hat{g}_L g_L}(m;t) \end{bmatrix} \otimes i(t) \tag{12}$$

Summing at the receiver, the scalar output of this realization is

$$R_{i\hat{g}_m R}(t) = \left(\mathbf{1}^T \times \mathbf{R}_{i\hat{g}_m R}(t)\right) = \sum_{\ell=1}^{L} C_{\hat{g}_\ell g_\ell}(m;t) * \ i(t). \tag{13}$$

C. **Green's Function Estimation**

The Green's function is an integral part of the two T/R receiver realizations. It can be estimated from a pilot signal measurement and is similar to the operations used for equalization[1,2], but is much better conditioned numerically for solution, since the forward, $g(r;t)$, rather than the inverse, $g^{-1}(r;t)$, is required for T/R. The estimated Green's function is used in the realizations to mitigate the distortion effects created by the medium and unknown transfer characteristics of the measurement system. For the multichannel case, we assume that the Green's functions can be estimated in transmitter-receiver pairs by transmitting the pilot signal from host array sensor to the client receiver, individually. Therefore, we discuss the channel-by-channel approach using a scalar algorithm to estimate the propagation matrix.

As mentioned previously, the estimate, $\hat{g}(r;t)$, can be obtained using the *optimal* Wiener[19,20] solution obtained from a pilot signal measurement by solving the minimum mean-squared error (MSE) problem leading to the optimal estimate for the ℓ^{th}-Green's function given by

$$\hat{\mathbf{g}}_{\ell} = \mathbf{C}_{pp}^{-1}(\ell)\mathbf{c}_{zp}(\ell); \quad \text{for} \quad \ell=1,\cdots,\mathrm{L}, \tag{14}$$

where $\mathbf{C}_{pp}$ is a $M \times M$ correlation matrix and $\mathbf{c}_{zp}$ is a $M \times 1$ cross correlation vector.

D. 1-bit T/R Receiver Implementation

Since the spatial information in the transmitted signal is essentially captured by the *phase* portion of the propagating wave ($g(\mathbf{r};t)$), the amplitude information is not as critical in utilizing the multipath. We developed a receiver that ignores or quantizes the amplitude and merely exploits the "phase-only" time reversed signals[18,21]. This is accomplished by recording the corresponding zero-crossings of the time-reversed signals quantized between ± 1 amplitudes establishing the 1-bit T/R receiver realizations[18]. This two-state system is commonly referred to as binary phase shift keying (BPSK) in the communications literature. The major advantage of such an implementation is that instead of requiring an expensive analog-to-digital (A/D) converter (e.g. 24-bits), a simple threshold switch can be used instead, since all that is required is to detect the zero-crossings. The disadvantage of this approach is increased quantization error and noise. That is, the noise will also be quantized to the ± 1 amplitudes and its inherent high frequency zero-crossings as well.

Although the 1-bit receiver design is simple in concept, it does introduce uncertainty into the processed data. Since 1-bit quantization is a *nonlinear* process, it is identical to a switch or relay in a physical system. The crudeness of 1-bit sampling introduces large quantization errors relative to the amplitude sampling. In fact the lower bound on quantization error indicates that the 1-bit design introduces 8 orders of magnitude larger deviations (errors) than the 24-bit design[1]. This error translates into an equivalent measurement noise decreasing the "in-band" (signal frequency bandwidth) SNR. The 1-bit quantization also acts as a strong amplifier of low amplitude data (usually noise) thereby reducing the overall processing gain. From the time-reversal perspective, it does offer a cost effective solution to phase sampling high frequency signals (EM, ultrasound) providing a mechanism to use T/R processing thereby increasing the overall spatial gain and coherence available at the receiver. This completes the discussion of the T/R receiver designs used as a compliment to pre-process the input for our time-reference modulation scheme to follow.

III. WIDEBAND T/R COMMUNICATIONS

In this section we discuss the development of a wideband T/R receiver design based on the concept of ultra wideband communications systems and the special modulation schemes associated with them. A communications system is deemed "wideband" based on its *fractional bandwidth*[22-24] that is defined as the ratio of its bandwidth and center frequency both specified by its high and low cutoff frequencies, that is,

$$BW_{\text{fractional}} \equiv \frac{BW}{f_{\text{center}}} \times 100 \ \ (\%) \tag{15}$$

where $BW = f_{\text{hi}} - f_{\text{lo}}$ is the transmission bandwidth and $f_{\text{center}} = \frac{f_{\text{hi}} + f_{\text{lo}}}{2}$ is the center (average) frequency with f_{hi}, f_{lo} the respective upper and lower –10 dB emission point frequencies. In standard ultra-wideband radio (electromagnetic transmissions) with typical center frequencies of $f_{\text{center}} > 2.5$ GHz need to have a –10 dB bandwidth of at least 500 MHz, while systems with $f_{\text{center}} < 2.5$ GHz need to have a fractional bandwidth of at least 20%. Such systems rely on short pulse waveforms that do *not* require sinusoidal carriers, since they can operate at baseband frequencies. In electromagnetics wideband transmissions have distinct advantages in communications[22-24].

Here we concentrate on taking advantage of the "carrier-free" modulation scheme called *time-reference modulation* that is based on transmitting narrow, modulating pulses and investigating the polarity of the resulting correlations. This scheme is closely related to the usual time-reversal procedures, since the autocorrelation process involves convolving the signal with its time-reversed replicant. Let us investigate the usual time-reference (*TRef*) modulation scheme first and incorporate the complimentary T/R receiver. The *TRef* design is basically a correlation-based receiver[22-24] that uses a pair of pulses per symbol: the first a pilot and the second the symbol. Since we are using a BPSK coding scheme, our symbol is the pulse multiplied by a ± 1 either preserving or inverting the pilot. Thus, the decoding process requires locating the pulse by *synchronizing* the receiver and using a priori knowledge of the inter-pulse timing intervals. The operations and timing of the *TRef* receiver are illustrated in Fig. 2. Here the received signal is delayed and correlated at the pre-specified *inter-pulse delay*, τ_{P}, within the *symbol time interval* (time segment) defined by τ_{S} ($\tau_{\text{S}} > \tau_{\text{P}}$) and then followed by a *polarity test* to determine the *sign*, σ. Consider the pulse pair (see Fig. 2)

$$i(t) = p(t) + \sigma\, p(t - \tau_{\text{P}}) \quad \text{for} \quad \sigma = \pm 1 \ \text{ and } \ \text{k}\tau_{\text{S}} < t \le (\text{k}+1)\tau_{\text{S}} \ \text{ with } k = 0, \ldots, K, \tag{16}$$

along with its delayed counterpart

$$i(t - \tau_{\text{P}}) = p(t - \tau_{\text{P}}) + \sigma\, p(t - 2\tau_{\text{P}}),$$

then the correlator output at τ_{P} is

$$C_{\text{ii}}(\tau_{\text{P}}) = \int_{t-\tau_{\text{P}}}^{t} i(\alpha) i(\alpha - \tau_{\text{P}}) d\alpha, \tag{17}$$

followed by the polarity test

$$\hat{\sigma} = \text{signum}\left[C_{\text{ii}}(\tau_{\text{P}})\right]. \tag{18}$$

The key to understanding the time-reference modulation operation is realizing that both the inter-pulse and symbol delays, $\{\tau_{\text{P}}, \tau_{\text{S}}\}$, are known a priori by the host and the clients; therefore, the received signal is delayed by τ_{P} and polarity tested over each subsequent τ_{S}-interval to extract the ± 1 bit. To see this confine the operation to an τ_{S}-interval so that Eq. (16) holds, then (1) perform the multiplication:

$$i(t)i(t-\tau_{\text{P}}) = p(t)\,p(t-\tau_{\text{P}}) + \sigma\, p(t-\tau_{\text{P}})\,p(t-\tau_{\text{P}}) + \sigma\, p(t)\,p(t-2\tau_{\text{P}}) + \sigma^2\, p(t-\tau_{\text{P}})\,p(t-2\tau_{\text{P}}),$$
$$\text{such that } k\tau_{\text{S}} < t \le (k+1)\tau_{\text{S}},\ k = 0, \cdots, K; \tag{19}$$

(2) perform the expectation to obtain:

$$C_{\text{ii}}(\tau_{\text{P}}) = E\left\{i(t)i(t-\tau_{\text{P}})\right\} = \sigma C_{\text{pp}}(0) + (1+\sigma^2)C_{\text{pp}}(\tau_{\text{P}}) + \sigma C_{\text{pp}}(2\tau_{\text{P}}), \tag{20}$$

and finally (3) test the polarity of $C_{\text{ss}}(\tau_{\text{P}})$ for a +1 or –1. If we assume that an impulse is selected for the pulse shape, then clearly the product of Eq. (19) is

$$C_{\text{ii}}(\tau_{\text{P}}) = E\left\{\delta(t)\delta(t-\tau_{\text{P}}) + \sigma\delta(t-\tau_{\text{P}})\delta(t-\tau_{\text{P}}) + \sigma\delta(t)\delta(t-2\tau_{\text{P}}) + \sigma^2\delta(t-\tau_{\text{P}})\delta(t-2\tau_{\text{P}})\right\},$$

which gives

$$C_{\text{ii}}(\tau_{\text{P}}) = E\left\{\sigma\delta(t-\tau_{\text{P}})\delta(t-\tau_{\text{P}})\right\} = \int_{t-\tau_{\text{S}}}^{t} \sigma dt = \sigma\tau_{\text{S}}. \tag{21}$$

So we see in the impulsive case, the receiver estimates the sign bit directly. In Fig. 3 we show the results for a gaussian pulse shape and code (+1, -1, -1, +1) with its recovery using the *TRef* receiver. Here in Fig. 3(a) we show the modulated code along with its delayed replicant in (b) and observe the correlation output with extracted code (point or impulse) used to determine the sign bit in (c). Note that it is only necessary to estimate the correlation value at τ_{P} within the τ_{S}-interval and determine its sign. We show the entire correlation function for completeness.

In the general case, the code is propagated through a medium causing a *propagation delay*, τ_{M}, as well; therefore, we model the *transmitted information sequence* (pulse train) as

$$i(t) = \sum_{k=0}^{K} p(t-\tau_{\text{M}}-k\tau_{\text{S}}) + \sigma\, p(t-\tau_{\text{M}}-\tau_{\text{P}}-k\tau_{\text{S}}) \quad \text{for} \quad k\tau_S < t \le (k+1)\tau_S. \tag{22}$$

Note also from this model the *synchronization* problem becomes that of estimating the propagation delay, $\hat{\tau}_{\mathrm{M}}$, from a controlled data set using the matched-filter approach[1,2].

Unfortunately, the complex medium also distorts the information sequence in both amplitude and phase, that is, the received signal is

$$z(t) = g(r;t) * i(t) \tag{23}$$

for $g(r;t)$ the spatio-temporal Greens function characterizing the medium as before. In this more realistic case, we see that the *TRef* output is therefore

$$C_{\mathrm{zz}}(t) = \left[g(r;t) * i(t) \right] * \left[g(r;\tau_{\mathrm{P}} - t) * i(\tau_{\mathrm{P}} - t) \right], \tag{24}$$

which can be expressed as

$$C_{\mathrm{zz}}(t) = \left[g(r;t) * g(r;\tau_{\mathrm{P}} - t) \right] * \left[i(t) * i(\tau_{\mathrm{P}} - t) \right] = C_{\mathrm{gg}}(\tau_{\mathrm{P}} - t) * C_{\mathrm{ii}}(\tau_{\mathrm{P}} - t), \tag{25}$$

from the commutivity property of the convolution operator. Clearly, the maximum is achieved at $t = \tau_{\mathrm{P}}$ giving the desired result. So we see that instead of observing the autocorrelation of the transmitted information sequence, we observe a distorted version resulting in the smearing of the code with the correlation function of the medium. Of course, noise contaminates this result as well[17,18].

One approach to remove these adverse effects is to use the T/R receiver in conjunction with the *TRef* modulation technique thereby mitigating the medium distortion and enhancing the information sequence for improved reception. This can be accomplished by focusing on-transmit via T/R I and II or passively on-receive via T/R III and IV. On transmission or reception the effect of time-reversal is to provide a processed input to the *TRef* receiver, that is,

$$z_{\mathrm{T/R}}(t) = z(t) * \hat{g}(r;-t) = C_{g\hat{g}}(t) * i(t). \tag{26}$$

A typical result for a gaussian windowed chirp pulse sequence is shown in Fig. 4. Here we see the result of propagating the sequence that was designed to match the channel bandwidth[17,18] through the highly reverberative medium. In Fig. 4(a) the transmitted pulse pair code sequence is shown along with the distorted received signal in (b). The result of the T/R pre-processing is shown in Fig.4(c) along with an expanded gaussian-windowed pulse. The *TRef* receiver then processes this data instead of the raw data increasing its performance to extract the code.

The basic operation of the overall T/R, *TRef* receiver design is illustrated in Fig. 5 where we observe the raw multichannel array input data pre-processed by the T/R

receiver. Synchronization is accomplished using the classical matched-filter with transmitted pulse replicant to estimate the propagation delay, τ_M. Once synchronized, the *TRef* receiver locates the code and quantizes to extract the sign bit of the BPSK sequence.

It is interesting to note that just as in classical detection theory[19], the value of the threshold is also selected for the receivers based on some performance criterion. We use a *symbol error criterion* to evaluate the performance of each of the receiver realizations in this paper. S*ymbol error* is defined as the percentage of symbols missed over the total transmitted. In our application, since a symbol is represented by one bit, symbol error is synonymous to bit error.

III. EXPERIMENTS

In this section we describe a variety of proof-of-principle experiments executed to evaluate the performance of the wideband designs. We investigate the performance of the various T/R receiver realizations (I-IV) used as pre-processors coupled to the *TRef* demodulation scheme. We discuss the results of the experiments demonstrating the performance of multichannel communications systems for both the 24-bit and 1-bit designs discussed previously in Sec. II D. As mentioned previously, we estimate the set of Green's functions of the environment for each transmitter-receiver pair. Using these Green's functions, we developed an experimental computer simulation for design and implementation of the various receivers.

We selected three experimental environments: (1) *stairwell*; (2) *short* tunnel/cave; and (3) *long* tunnel/cave. For comparative purposes, the stairwell is that used in previous narrowband designs[17,18], while the short and long tunnel experiments were selected to investigate the wideband receiver designs in a highly reverberative environment that has a variety of applications including robot communications in a confined environment, military operations in caves and tunnels as well as tunnel mapping.

With this motivation in mind, we discuss the experimental environment and processing to gather the data from the *TRef* receiver using the T/R pre-processor. We have already addressed the steps required to extract the coded information sequence using the various T/R receiver realizations coupled to the *TRef* modulation scheme in the previous section.

The basic experimental approach is summarized (see Fig. 5):

1. *transmit* the pilot signal, that is, excite the medium with a gaussian-windowed chirp pulse (pilot) signal to estimate the set of Green's functions;
2. *transmit* the pulse-pair coded information signals from the host source array (speakers) along with the required Green's functions (T/R I and II), measured pilot signal, etc. through the reverberant medium to the microphone receiver;
3. *receive* (client microphone) the noisy, reverberant signal and digitize;
4. *pre-process* the raw data with the T/R receiver realizations (software);

5. *synchronize* the processed data using a matched-filter processor to estimate the temporal onset of the code (propagation delay);
6. *locate* the code by demodulating it with the *TRef* receiver; and
7. *quantize* the code using the polarity test and extracting it from the demodulated data for performance analysis.

We used the identical equipment for each of the subsequent experiments with time-reference (correlation-based) modulation for the wideband case and compared the results to the previous narrowband amplitude modulated designs[17,18]. The array-to-point (host array-to-client) experiments were performed using Meyer Sound, MM-4, 4" single element speakers configured in an 8-element vertical array with a 6" pitch powered by a Crown Audio CTS 8200, 8-channel, 150 watt amplifier and a Data Physics, DP-703 arbitrary waveform generator/digitizer for transmitting both the gaussian-windowed (23.4ms duration) chirp pulse (pilot) swept from 0.6 to 1.8kHz corresponding to a 50% fractional bandwidth. The corresponding signed BPSK code pulse with an inter-pulse spacing of 23.4ms (τ_P) was designed to ensure non-overlapping code pulses while the symbol period (τ_S) associated with the transmission of 78.1ms ensured adequate temporal symbol separation and integration time for the polarity tests. On reception, B&K 4935, ¼"-microphones are used in an 8-element receiver array along with the 24-bit Data Physics digitizer sampling at 12.8kHz. We use two, 8-element, linearly-spaced (6" pitch), vertical arrays to construct the host array: one for transmission consisting of the eight speakers and one for reception consisting of the eight microphone receivers. Individual speakers and microphones are positioned at each client station in the reverberative environment. The experiment is controlled using a laptop computer. The transmitted code, the gaussian-windowed chirp of Fig. 4, was received on a client microphone. As observed in the figure, the measurement is dominated by a long reverberation response and noise.

For our receiver performance analysis, we use the symbol (bit) error criterion[17]. We determine the symbol error by varying the threshold at the processed receiver output and determine the number of symbols missed at that threshold. The performance function (% symbol error versus threshold) is "U-shaped" with the base of the "U" residing in the *zero-symbol error* region (e.g. see Fig. 6 for *TRef* I). Of particular interest is the percentage of the threshold interval corresponding to the zero-symbol error region *relative* to the *total* threshold interval (-1 to +1) evaluated. We use this threshold interval percentage to provide a metric for evaluating the robustness of the particular receiver design. The *higher* the percentage, the larger the threshold interval corresponding to zero-symbol error and therefore the more robust the design. We compared all of the receiver designs and a bar chart with these percentages listed is illustrated in Figs. 12-14. We also calculated the percentage threshold intervals for each realization using both 24-bit and 1-bit designs.

A. Stairwell Experiments and Results

As before[17,18], the first set of experiments was performed in a stairway located between two floors consisting of three landings, high ceilings of corrugated steel, pipes,

handrails and other non-sound absorbing protrusions as well as ambient building noise. Details of the experiment were discussed previously in References 17 and 18 clearly demonstrating a highly reverberant environment.

For the stairwell, client receiver No. 1 is located at the middle landing, while client receiver No. 2 is at the top landing as before. Note that client No. 1 has a higher SNR than that at client No. 2 due to the direct path. After obtaining the set of Green's functions for each client receiver, we investigate the following cases: (1) focused transmission to each client receiver, *individually* and checked the other (non-focused) client receiver station for leakage of the cross-correlation functions; and (2) repeated experiments for 1-bit realizations. For each of the T/R I and II receivers (focus on transmit), we focused on the individual client receiver stations and evaluated their performance, while T/R III and IV receivers (focus on receive) were also evaluated.

TRef I Receiver Performance:

The realization of this *TRef I* receiver (see Fig. 2) uses the estimated set of Green's functions from the array sensors convolved with the code *transmitted* into the stairwell[6,7]. This is a common realization that has been applied in the literature[17-18]. After T/R pre-processing, synchronization and demodulation, we see the corresponding information code estimates produced from the output of the *TRef I* receiver in Fig. 6. For each client receiver the 24-bit and 1-bit designs (upper row) are illustrated using solid lines. This code estimate is down-sampled to the symbol rate and then quantized based on a selected threshold. Each estimated symbol (O) is then compared to the true transmitted symbol (*) that is overlaid in the figure for illustrative purposes. For *TRef I*, it is clear that raw coded information pulses are discernable at the receiver output data (solid line) that the pre-processed data tracks the "true" code. Since all of the symbols estimated by *TRef I* quantizer perfectly match those transmitted, the BPSK information code is captured with zero-symbol error for the selected threshold. Note also the high SNR achieved through T/R focusing and inherent array gain compared to the previous narrowband experiments reported on previously[17,18]. It is also interesting to note that the 1-bit designs at each client have deteriorated compared to the 24-bit design. This performance is expected due to increased quantization noise.

By varying the threshold over the entire T/R receiver estimate, the performance U-curve (% symbol error versus threshold) is generated as shown in Fig. 6 (lower row). This curve plays a role similar to the operating characteristic curve[19] in classical detection theory---thresholds can be selected to minimize symbol error. As mentioned previously, the length or range of the threshold interval yielding zero-symbol error compared to the total range gives an indication of the performance capability of the receiver. Each receiver is compared in the bar charts of Figs. 12-14. The interesting property is that it is possible to find a threshold interval yielding zero-symbol error indicating the robustness of the receiver, that is, the larger the interval, the more threshold values can be selected to yield zero-symbol error. The performance on this data is as expected, some robustness is sacrificed as the cost of simplicity using the 1-bit designs. Examining the U-curves, we see that the receiver is able to achieve approximately a 72% threshold interval using the

24-bit design, while the interval decreases significantly to 43% using the 1-bit design. The 1-bit design captures the spatial information by using the zero-crossings of *both* signal and noise eliminating the amplitude information. When noise only is quantized, it has an amplitude level of ±1. The inherent in-band signal and noise have now also been quantized to the *same* level thereby causing the observed performance degradation.

TRef III Receiver Performance:

This *TRef III* receiver uses the estimated set of Green's functions convolved with the raw received code data on *reception*. The results of the performance of this realization are shown in Fig. 7. After the T/R pre-processing, the experimental results track the transmitted code as before. For the selected threshold, zero-symbol error is achieved with perfect code recovery. In the figure we observe the outstanding performance of the 24-bit (80% zero-symbol error threshold interval) and the degraded performance of the 1-bit (28% threshold interval) designs (upper row). The overall performance is also shown in the lower row of the figure where we observe the U-shaped symbol error curves. The performance of this receiver is quite good; however, we note the significant performance degradation in the 1-bit design due to the inherent quantization errors.

Overall Stairwell Performance

Next we compare the overall robustness performance of each design at the individual client stations for both 24-bit and 1-bit designs shown in Figs. 12 and 13. We illustrate the performance by bar charts with the height of the bar determined by the % threshold range occupied by zero-symbol error of the corresponding U-curve. In Fig. 12 the 24-bit design chart shows a significant performance improvement over previous point designs[6,7] with the average wideband range over 72% (client 1) and 77% (client 2) of the total threshold interval for zero-symbol error compared to the narrowband designs with just over 48% (client 1) and 44% (client 2) illustrating that the *TRef* design coupled with the T/R pre-processor is quite capable of operating effectively in a highly reverberative environment with improved performance. This improvement appears to be true for the 1-bit realizations except for client 2 using T/R III and IV pre-processing. The average wideband range has degraded somewhat to 70% for client 1 and severely to 34% for client 2, while the narrowband realizations were at 56% and 32%, respectively. Even though the wideband realizations are an improvement over the narrowband for the 1-bit receivers on the average, the poor individual performances of *TRef III* and *IV* are troublesome. The cause in the 1-bit case is usually a significant loss in signal levels creating higher quantization errors. However, it still appears reasonable to conclude that the wideband designs using the *TRef* receiver with the T/R pre-processors demonstrate an improved overall performance over the narrowband designs.

B. Tunnel/Cave Experiments and Results

The second set of experiments was performed in the tunnel-like environment shown in Fig. 8 where we see the structure that is actually part of an underground

accelerator complex located at the Lawrence Livermore National Laboratory. It consists of a series of bends, corners and turns with ancillary equipment and racks as well as varying ceiling heights throughout. Large concrete and steel doors are present for radiation protection when the accelerator is activated. The *short* tunnel consists of 130' long run stretch with major bends and severe 90^{o} turn while the *long* tunnel consists of the short tunnel extended for an overall length of 180' with the receiver located in a heavily shielded laboratory including large and noisy equipment (generators, coolers, air conditioners, fans, etc.) with concrete walls and the large concrete/steel door for radiation isolation. All of these tunnel-like obstructions contribute significantly creating an extremely hostile, highly reverberative environment. The figure illustrates the various parts of the tunnel-like environment along the communications path.

The *TRef* receivers *I* and *III* were implemented using the T/R processor as before under the same propagation and transmission/reception conditions used in the stairwell ($\tau_{\mathrm{P}}, \tau_{\mathrm{S}}$), gaussian-windowed chirp, etc. as before. The *short* tunnel results are shown in Figs. 9 and 10. *TRef I* performance is illustrated in Fig. 9 yielding a 73% zero-symbol error threshold interval with the 24-bit scheme, similar to the *stairwell* performance, with the 1-bit design deteriorating to a 38% threshold interval indicating the sensitivity of the design to quantization errors contributed to the significant loss in SNR created by the obstructions and the length of the propagation paths.

The *short* tunnel results for *TRef III* are shown in Fig. 10 where we observe a 73% threshold interval for the 24-bit design with a severe deterioration of performance for the 1-bit design of 20% threshold interval. It appears that the wideband design suffers more significant degradation for the 1-bit designs than the narrowband case due to the decreased signal levels created by propagation losses and therefore increased quantization errors. Also the amount of in band noise is intrinsically larger for the wide band case.

The final set of experiments is shown in Fig. 11 for the *long* tunnel designs of *TRef III*. Here we again observe degradation in overall performance to 68% for the 24-bit design and a 26% zero-symbol error threshold interval for the 1-bit design. Again this is not unexpected due to the propagation losses and ensuing quantization errors.

These results imply that the longer the tunnel, the more propagation losses contribute to a significant decrease in SNR at the receiver. Therefore, the robust performance of the receivers suffer performance degradations especially for the 1-bit designs, that is, the zero-symbol error threshold intervals decrease significantly. As demonstrated, the 1-bit designs are much more sensitive to these losses than in previous studies[7]. This follows since decreasing signal levels increases the in-band noise and uncertainty leading to much large quantization errors and therefore severe deterioration of the receiver performance even using the T/R pre-processing for enhancement.

Overall Tunnel Performance

The overall performance of the wideband *TRef* processor for both the *short* and *long* tunnel environments are show in the bar chart of Fig. 13 with the % zero-symbol error threshold range shown as before for the stairwell. The chart displays both the 24-bit and 1-bit realizations. The 24-bit *short* and *long* tunnel experimental results are quite good with an average threshold range of 75% and 67%, respectively. This slight decrease in the long tunnel is expected because of the lower SNR due to propagation losses caused by its extended length and obstructions. However, the 1-bit results are somewhat disappointing with an average threshold range of less than 10% for the short tunnel and 25% for the long. Again *TRef III* and *IV* demonstrating poor individual performance. Overall the 24-bit *TRef* receiver performance is quite good for both tunnel experiments, while the 1-bit realizations are just marginal comparatively. It is interesting to note that the 1-bit performance is better for longer tunnel than the shorter tunnel. This might be caused by a decrease in ambient noise at the position of the microphone for the long tunnel.

IV. CONCLUSIONS

In this paper we have discussed the development of a multichannel wideband time-reference (*TRef*) or correlation-based receiver using a time-reversal (T/R) pre-processor to enhance and extract an information sequence transmitted through highly reverberative media. We have evaluated the performance of this design in a well-known stairwell that was used for narrowband designs previously[17,18] and compared the overall results. This effort, therefore, extends the previous narrowband results to the wideband case and explores communications in tunnel-like structures that are important in a variety of applications.

We discussed the performance of the multichannel, wideband receiver designs in the highly reverberative stairwell demonstrating that the performance was comparable by achieving the same level of performance using the % zero-symbol error metric. We also showed that the wideband receiver designs could be deployed effectively in a tunnel-like environment of an accelerator facility at the Lawrence Livermore National Laboratory. Again the performance was quite comparable to that expected of a narrowband system, but somewhat surprisingly the 1-bit receiver realizations degraded significantly over the past work[17,18]. It was conjectured that the elongated acoustic propagation paths causing large signal attenuation was the underlying catalyst increasing the significance of the 1-bit quantization errors.

More specifically, the wideband *TRef* receiver realization with the T/R pre-processor demonstrated superior performance to the previous narrowband designs in all of the 24-bit experiments; however, the 1-bit wideband designs were just marginally better or equivalent to the narrowband case. From these results we conclude that coupling the T/R pre-processor to a wideband *TRef* modulation receiver not only simplifies the synchronization problem, but clearly improves the overall communication system performance in a highly reverberative environment. We also conclude that the *TRef*

processor is capable of performing well in tunnel-like environments providing an effective method of communication.

Future work in this area is based on applying these results especially the 1-bit realizations to the electromagnetic case for wireless communications.

ACKNOWLEDGEMENTS

This work was performed under the auspices of the U. S. Department of Energy by UC, Lawrence Livermore National Laboratory under Contract No. W-7405-Eng-48.

REFERENCES

[1] J. G. Proakis, *Digital Communications.* (McGraw-Hill, New York, N.Y., 1995).

[2] S. Haykin, *Communication Systems.* (John Wiley, New York, N.Y., 2001).

[3] M. Fink, "Time reversal in acoustics," Contemporary Physics., vol. 37, (2) pp. 95-109, (1996).

[4]D. H. Chambers, J. V. Candy, S. K. Lehman, J. S. Kallman, A. J. Poggio and A. W. Meyer, "Time-reversal and the spatio-temporal matched-filter," *J. Acoust. Soc. Am.*, **116**, (3), pp. 1348-1350, (2004).

[5] A. Parvulescu, "Matched-signal (MESS) processing by the ocean," *J. Acoust. Soc. Am.*, **98**, (2), p. 943-960, (1995).

[6] D. R. Jackson and D. R. Dowling, "Phase conjugation in underwater acoustics," *J. Acoust. Soc. Am.*, **89**, (1), p. 171-181, (1991).

[7] D. R. Dowling, "Acoustic pulse compression using passive phase-conjugate processing," *J. Acoust. Soc. Am.*, **95**, (3), p. 1450-1458, (1994).

[8] J-P Hermand and W. Roderick, "Acoustic model-based matched filter processing for fading time-dispersive ocean channels: Theory and experiment," *IEEE J. Oceanic Engr.*, Vol. 18, No. 4, p. 447-465, (1993).

[9] R. K. Brienzo and W. S. Hodgkiss, "Broadband matched-field processing," *J. Acoust. Soc. Am.*, **94**, (5), p. 2821-2831, (1993).

[10] W. A. Kuperman, W. S. Hodgkiss and H. C. Song, "Phase conjugation in the ocean: Experimental demonstration of an acoustic time-reversal mirror," *J. Acoust. Soc. Am.*, **103**, (1), p. 25-40, (1998).

[11] J-P Hermand, "Broad-band geoacoustic inversion in shallow water from waveguide impulse response measurements on a single hydrophone: theory and experimental results," *IEEE J. Oceanic Engr.*, Vol. 24, No. 1, p. 41-66, (1999).

[12] W. S. Hodgkiss, H. C. Song, W. A. Kuperman, T. Akal, C. Ferla and D. R. Jackson, "A long range and variable focus phase-conjugation experiment in shallow water," *J. Acoust. Soc. Am.*, **105**, (3), p. 1597-1604, (1999).

[13] G. Edelmann, T. Akal, W. S. Hodgkiss, S. Kim, W. A. Kuperman and H. C. Song, "An initial demonstration of underwater acoustic communication using time reversal," *IEEE J. Oceanic Engr.*, Vol. 27, No. 3, p. 602-609, (2002).

[14] D. Rouseff, D. R. Jackson, W. L. Fox, C. D. Jones, J. A. Ritcey and D. R. Dowling, "Underwater acoustic communication by passive-phase conjugation: theory and experiment," *IEEE J. Oceanic Engr.*, Vol. 26, No. 4, p. 821-831, (2001).

[15] K. B. Smith, A. M. Abrantes and A. Larraza, "Examination of time-reversal acoustics in shallow water and applications to noncoherent underwater communications," *J. Acoust. Soc. Am.*, **113**, (6), p. 3095-3110, (2003).

[16] M. Heinemann, A. Larraza and K. B. Smith "Experimental studies of applications of time-reversal acoustics to noncoherent underwater communications," *J. Acoust. Soc. Am.*, **113**, (6), p. 3111-3116, (2003).

[17] J. V. Candy, Alan W. Meyer, A. J. Poggio and B. L. Guidry, "Time-reversal processing for an acoustic communications experiment in a highly reverberant environment," *J. Acoust. Soc. Am.*, **115**, (4), pp. 1621-1631, (2004).

[18] J. V. Candy, A. J. Poggio, D. H. Chambers, B. L. Guidry, Christopher L. Robbins, and Claudia A. Kent, "Multichannel time-reversal processing for acoustic communications in a highly reverberant environment," *J. Acoust. Soc. Am.*, **118**, (4), pp. 2339-2354, (2005).

[19] D. H. Johnson and D. E. Dudgeon, *Array Signal Processing: Concepts and Techniques*, (Prentice-Hall, Engelwood Cliffs, New Jersey, 1993).

[20] J. V. Candy, *Model-Based Signal Processing*. (Wiley/IEEE Press, Hoboken, New Jersey, 2006).

[21] A. Derode, A. Tourin and M. Fink, "Ultrasonic pulse compression with one-bit time reversal through multiple scattering," *J. Appl. Phys.* **85,** 6343.

[22] Linqing Yang and G. B. Giannakis, "Ultra-wideband communications," *IEEE Signal Processing Magazine*, vol. 21, No. 6, pp. 26-54, (2004).

[23] A. F. Naguib, N. Seshadri and A. R. Calderbank, "Space-time coding and signal processing for high data rate wireless communications," *IEEE Signal Processing Magazine*, vol. 17, No. 3, pp. 76-92, (2000).

[24] A. J. Paulraj and C. B. Papadias, "Space-time processing for wireless communications," *IEEE Signal Processing Magazine*, vol. 14, No. 6, pp. 49-83, (1997).

#####

[16] S. Yon, M. Tanter and M. Fink, "Sound focusing in rooms: The time-reversal approach," *J. Acoust. Soc. Am.,* **113**, (3), p. 1533-1543, (2003).

[26] Thomas Folégot, Julien de Rosny, Claire Prada, and Mathias Fink, "Adaptive instant record signals applied to shallow water detection," *J. Acoust. Soc. Am.* **115**, 2468 (2004)

[27] Thomas Folegot, Philippe Roux, William A. Kuperman, William S. Hodgkiss, Hee Chun Song, Tuncay Akal, and Mark Stevenson, "Using acoustic orthogonal signals in shallow water time-reversal applications," *J. Acoust. Soc. Am.* **115**, 2468 (2004).

[28] Heechun Song, W. S. Hodgkiss, W. A. Kuperman, Philippe Roux, T. Akal, and M. Stevenson, "Simultaneously multiple-depth coherent communications using time reversal," *J. Acoust. Soc. Am.* **115**, 2467 (2004).

[29] George Papanicolaou, "Remote sensing and communications in random media," *J. Acoust. Soc. Am.* **113**, 2212 (2003).

[30] Geoffrey F. Edelmann, Seongil Kim, W. S. Hodgkiss, W. A. Kuperman, H. C. Song, and Tuncay Akal, "Combining and comparing time reversal processing and adaptive channel equalization for communication sequences," *J. Acoust. Soc. Am.* **112**, 2447 (2002).

[31] Joseph A. Root and Peter H. Rogers, "Performance of an underwater acoustic volume array using time-reversal focusing," *J. Acoust. Soc. Am.* **112**, 1869 (2002).

[32] M. Tanter, J-L. Thomas and M. Fink, "Time-reversal and the inverse filter," *J. Acoust. Soc. Am.,* **108**, p. 223-234, (2000).

[33] P. Blomgren and G. Papanicolaou, "Super-resolution in time-reversal acoustics," *J. Acoust. Soc. Am.,* **111**, (1), p. 230-248, (2002).

[34] A. Derode, A. Tourin, J. de Rosny, M. Tanter, S. Yon and M. Fink, "Taking advantage of multiple scattering to communicate with time-reversal antenna," *Phys. Rev. Ltrs.,* Vol. 90, No. 1, p. 014301-1 to 014301-4, (2003).

FIGURE CAPTIONS
For
Wideband multichannel time-reversal processing for acoustic communications in a tunnel-like structure
Candy et. al.

FIG. 1. The basic communications problem: Host array transmission to client receiver stations through propagation channel (medium). The basic environment including the host transmitter/receiver, hostile medium along with the corresponding sets of Green's functions transmitter-receiver pairs from host array to client receiver stations in the communications network array.

FIG. 2. Time-reference receiver: reception (raw or processed data); inter-pulse delay (τ_P), reversal, correlation and polarity (sign) test for code extraction.

FIG. 3. Time-reference receiver demodulation: (a) transmitted gaussian pulse coded pairs. (b) Inter-pulse delayed, τ_P , sequence. (c) Correlation output with recovered sign bits (dashed impulses) from polarity testing.

FIG. 4. T/R pre-processing for gaussian-windowed chirp in a reverberative stairwell medium: (a) Transmitted pulse pair (code) sequence. (b) Raw received data. (c) T/R pre-processed data for input to *TRef* demodulator. (d) Zoomed gaussian-window pulse estimation.

FIG. 5. *TRef* receiver with complimentary T/R processing: raw multichannel array input data, T/R pre-processor, matched-filter synchronizer, *TRef* demodulator and quantizer to extract the code.

FIG. 6. Multichannel *TRef I* receiver output coded estimates (solid line) using the T/R I pre-processor in *stairwell*: Coded estimates (solid line) along with true BPSK code sequence (dashed line) for 24-bit and 1-bit (upper row) designs at each client receiver for true symbols (*) and estimated symbols (O) yielding a zero-bit error performance for the selected threshold. Performance U-curves for focusing at client one using 24-bit (73% zero-symbol error threshold interval) and 1-bit (43% threshold interval) designs. The degradation of the 1-bit design is 30% threshold interval.

FIG. 7. Multichannel *TRef III* receiver output coded estimates (solid line) using the T/R III pre-processor in *stairwell*: Coded estimates (solid line) along with true BPSK code sequence (dashed line) for 24-bit and 1-bit (upper row) designs at each client receiver for true symbols (*) and estimated symbols (O) yielding a zero-bit error performance for the selected threshold. Performance U-curves for focusing at client one using 24-bit (80% zero-symbol error threshold interval) and 1-bit (20% threshold interval) designs. The degradation of the 1-bit design is 60% threshold interval.

FIG. 8. Experimental environment and setup for T/R communications testing: tunnel layout with blind hallways and high corrugated steel ceilings (10-20') along with the equipment set-up for array-to-point communications. Note that a schematic map demonstrates the tunnel communications path with the client receiver is approximately 180' from host array.

FIG. 9. Multichannel *TRef I* receiver output coded estimates (solid line) using the T/R I pre-processor in *short tunnel* (~130'): Coded estimates (solid line) along with true BPSK code sequence (dashed line) for 24-bit and 1-bit (upper row) designs at each client receiver for true symbols (*) and estimated symbols (O)

yielding a zero-bit error performance for the selected threshold. Performance U-curves for focusing at client one using 24-bit (73% zero-symbol error threshold interval) and 1-bit (33% threshold interval) designs. The degradation of the 1-bit design is 40% threshold interval.

FIG. 10. Multichannel *TRef III* receiver output coded estimates (solid line) using the T/R III pre-processor in *short tunnel* (~130'): Coded estimates (solid line) along with true BPSK code sequence (dashed line) for 24-bit and 1-bit (upper row) designs at each client receiver for true symbols (*) and estimated symbols (O) yielding a zero-bit error performance for the selected threshold. Performance U-curves for focusing at client one using 24-bit (75% zero-symbol error threshold interval) and 1-bit (9% threshold interval) designs. The degradation of the 1-bit design is 66% threshold interval.

FIG. 11. Multichannel *TRef III* receiver output coded estimates (solid line) using the T/R III pre-processor in *long tunnel* (~180'): Coded estimates (solid line) along with true BPSK code sequence (dashed line) for 24-bit and 1-bit (upper row) designs at each client receiver for true symbols (*) and estimated symbols (O) yielding a zero-bit error performance for the selected threshold. Performance U-curves for focusing at client one using 24-bit (68% zero-symbol error threshold interval) and 1-bit (25% threshold interval) designs. The degradation of the 1-bit design is 43% threshold interval.
(Jim: The solid line for the true BPSK code sequence does not extend all the way across the 1-bit receiver output)

FIG. 12. *TRef I-IV* wideband receiver overall performance in *stairwell* using T/R pre-processor based on the threshold range (% of total) for zero-symbol error threshold interval performance at both client stations for 24-bit designs. The narrowband designs from previous work[18] are included for comparison.

FIG. 13. *TRef I-IV* wideband receiver overall performance in *stairwell* using T/R pre-processor based on the threshold range (% of total) for zero-symbol error threshold interval performance at both client stations for 1-bit designs. The narrowband designs from previous work[18] are included for comparison.

FIG. 14. *TRef III-IV* receiver performance in *short (~130')* and *long tunnels (~180')* using T/R pre-processor based on the threshold range (% of total) for zero-symbol error threshold interval performance at both client stations for both 24-bit and 1-bit designs.

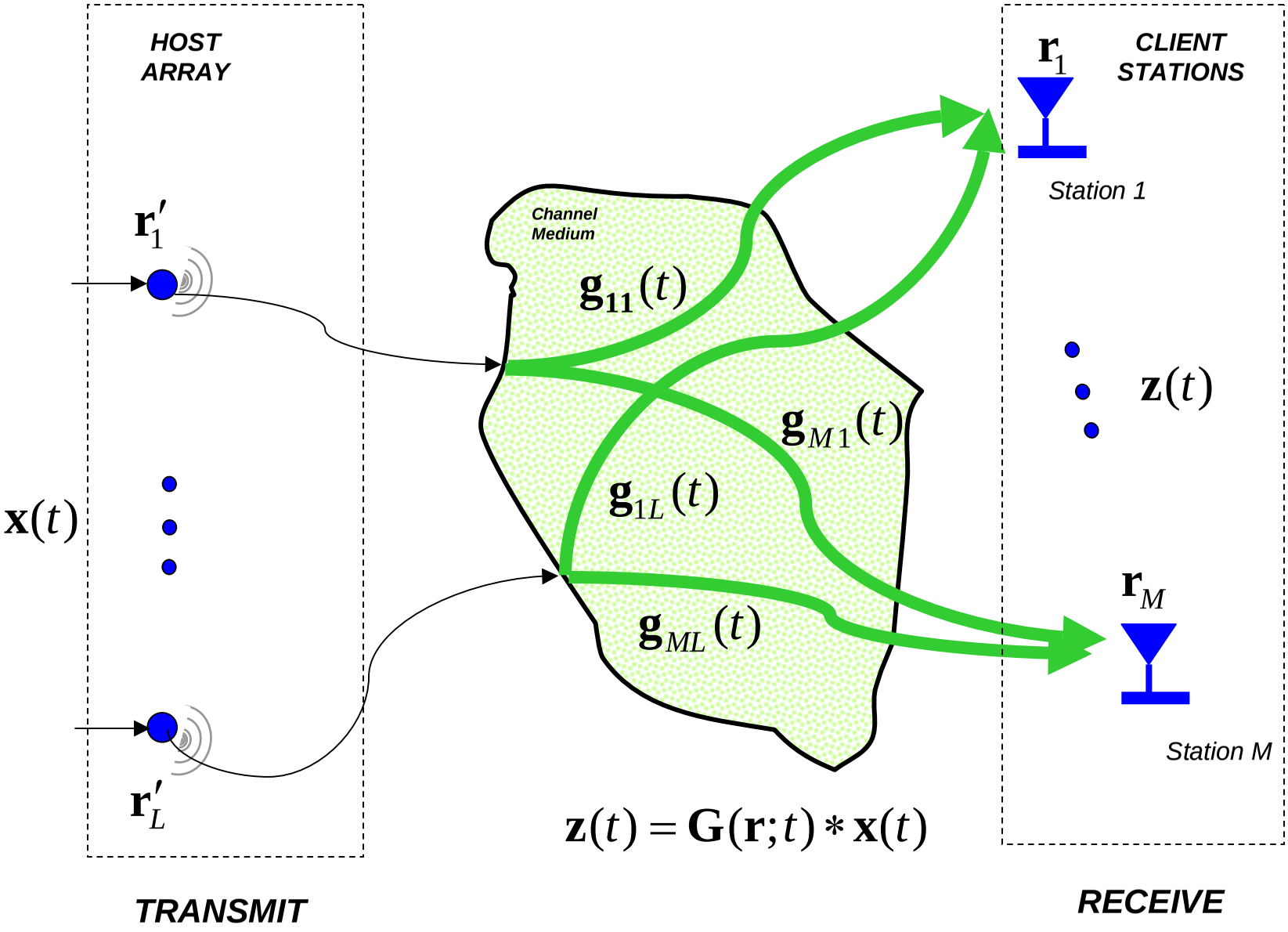
HOST
ARRAY
$\mathbf{r}'_1$
$\mathbf{x}(t)$
$\mathbf{r}'_L$
TRANSMIT
Channel
Medium
$\mathbf{g}_{11}(t)$
$\mathbf{g}_{M1}(t)$
$\mathbf{g}_{1L}(t)$
$\mathbf{g}_{ML}(t)$
$\mathbf{z}(t) = \mathbf{G}(\mathbf{r};t) * \mathbf{x}(t)$
$\mathbf{r}_1$
CLIENT
STATIONS
Station 1
$\mathbf{z}(t)$
$\mathbf{r}_M$
Station M
RECEIVE

F1

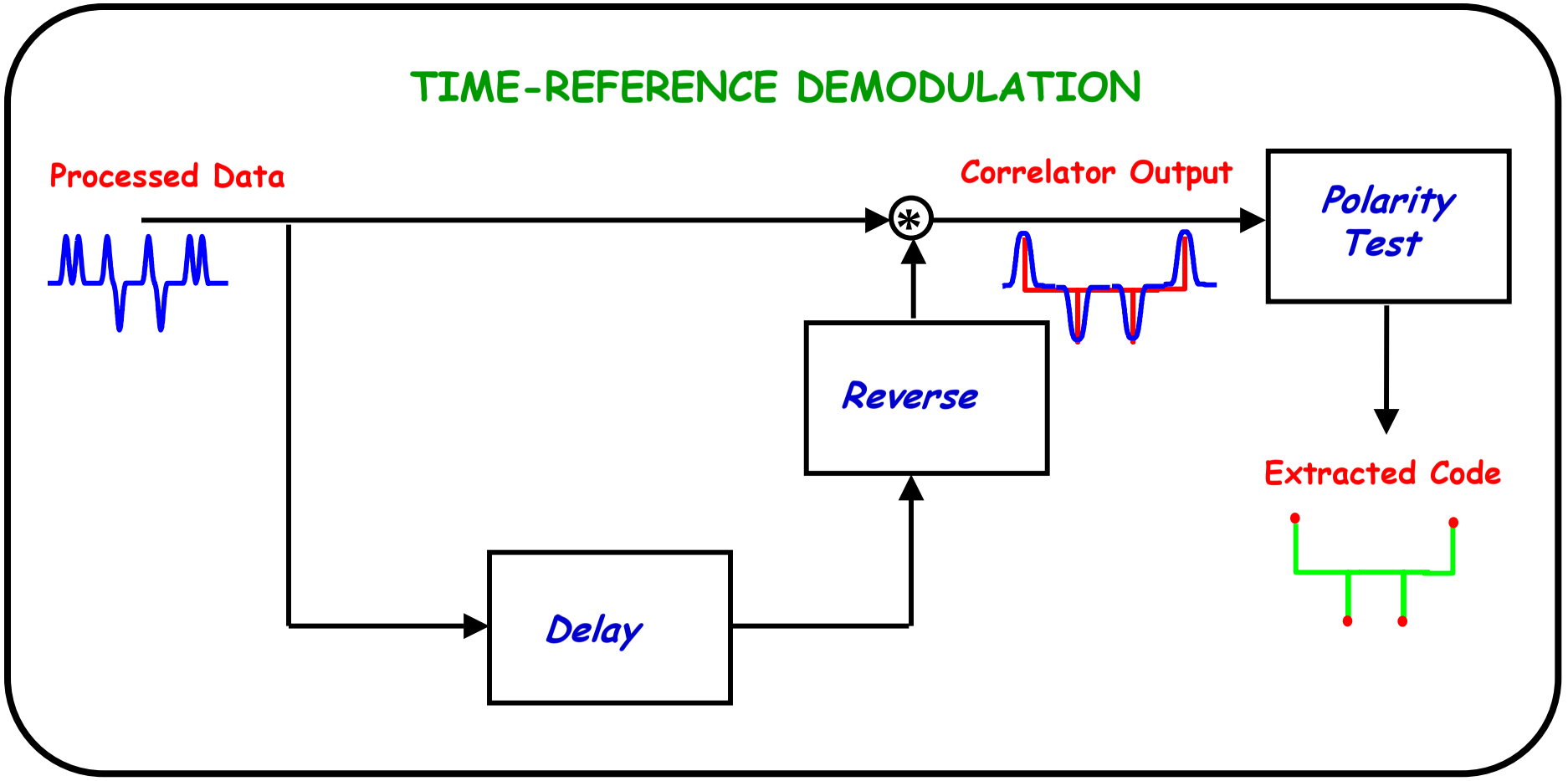
TIME-REFERENCE DEMODULATION
Processed Data
Correlator Output
Polarity Test
Reverse
Extracted Code
Delay

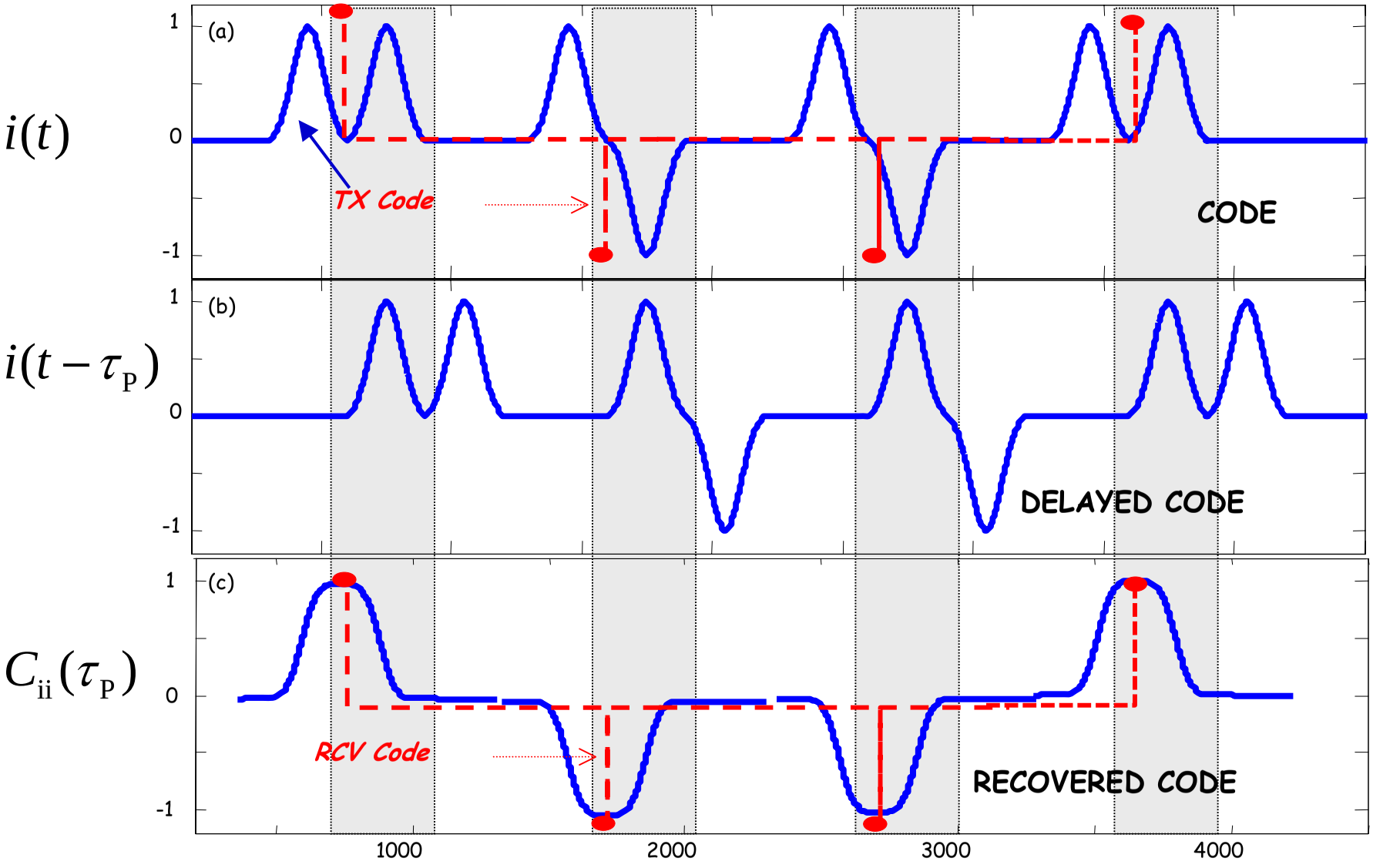
$i(t)$
$i(t-\tau_P)$
$C_{ii}(\tau_P)$
(a)
(b)
(c)
1
0
-1
TX Code
CODE
DELAYED CODE
RCV Code
RECOVERED CODE
1000
2000
3000
4000

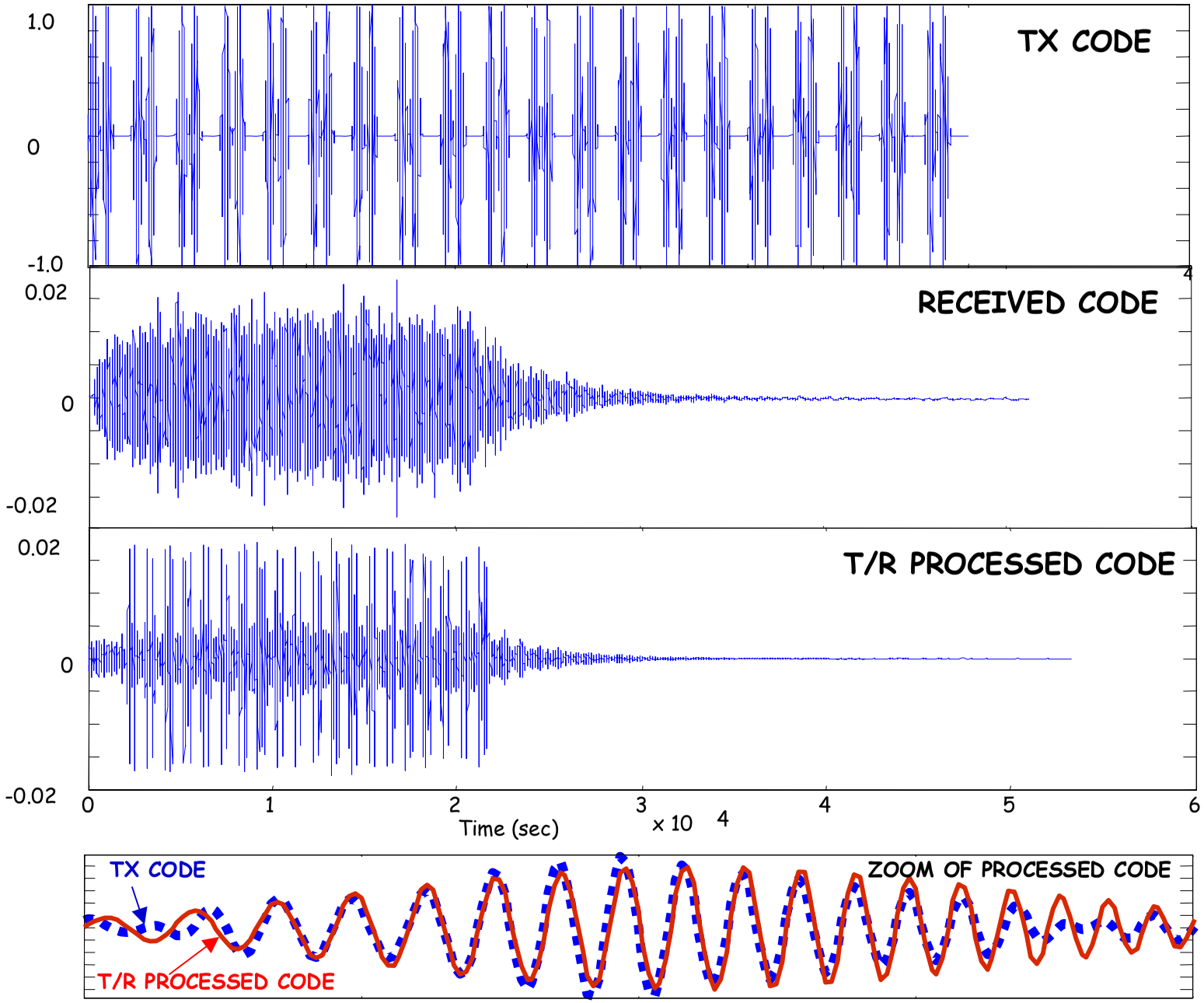
TX CODE
RECEIVED CODE
T/R PROCESSED CODE
1.0
0
-1.0
0.02
0
-0.02
0.02
0
-0.02
0
1
2
3
4
5
6
Time (sec)
x 10 4
TX CODE
T/R PROCESSED CODE
ZOOM OF PROCESSED CODE

WIDE BAND T/R RECEIVER PROCESSING

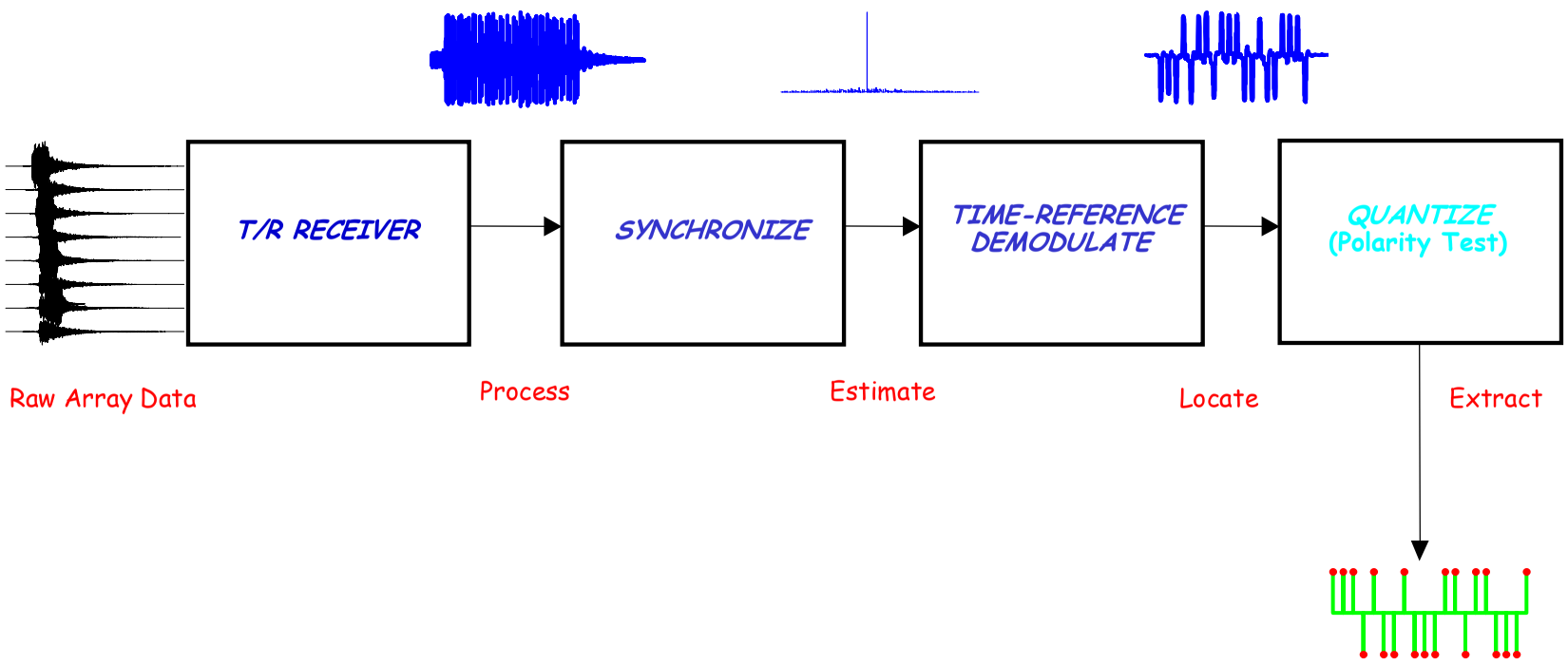

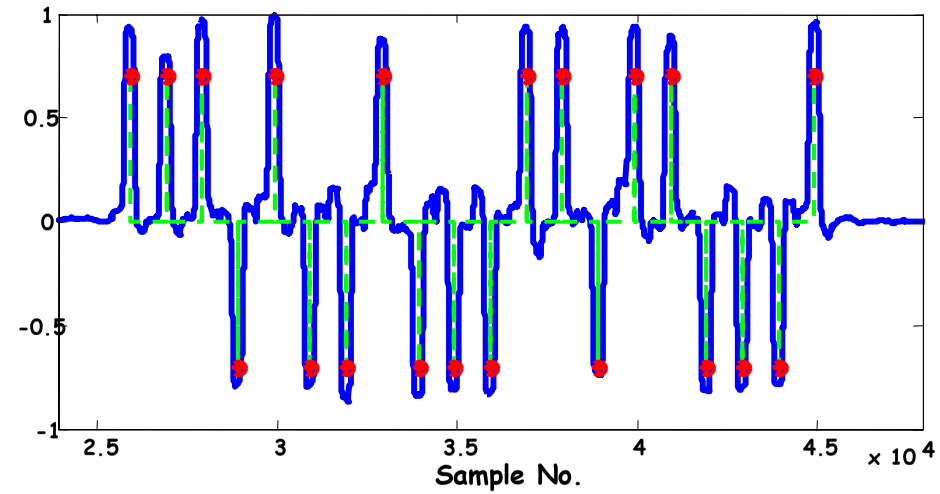
1
0.5
0
-0.5
-1
2.5
3
3.5
4
4.5
× 10 4
Sample No.

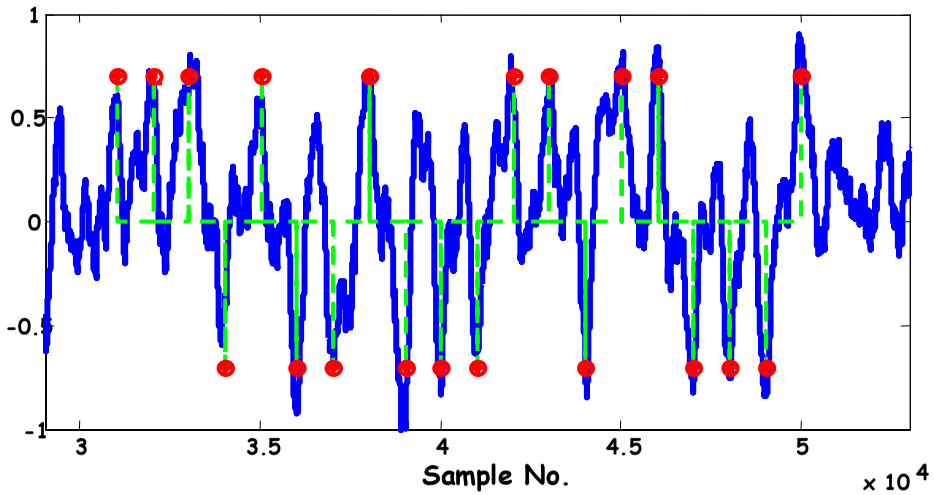
1
0.5
0
-0.5
-1
3
3.5
4
4.5
5
× 10 4
Sample No.

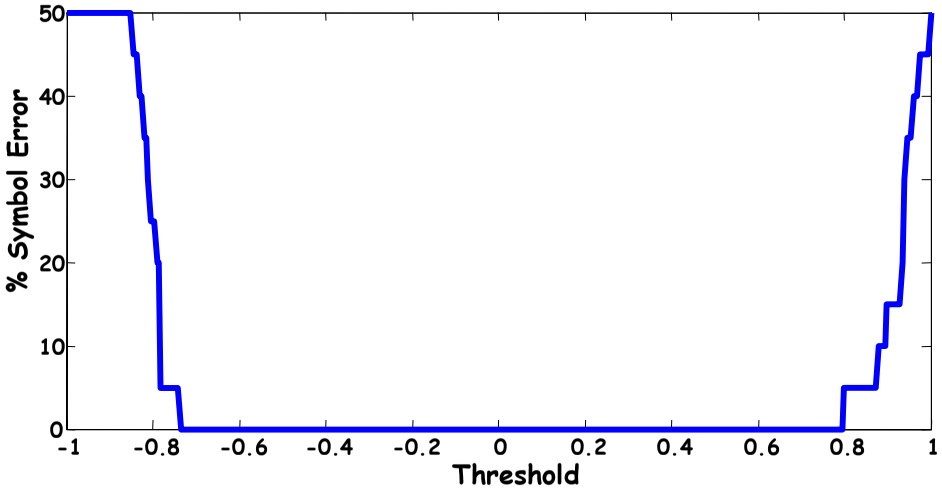
% Symbol Error
50
40
30
20
10
0
-1
-0.8
-0.6
-0.4
-0.2
0
0.2
0.4
0.6
0.8
1
Threshold

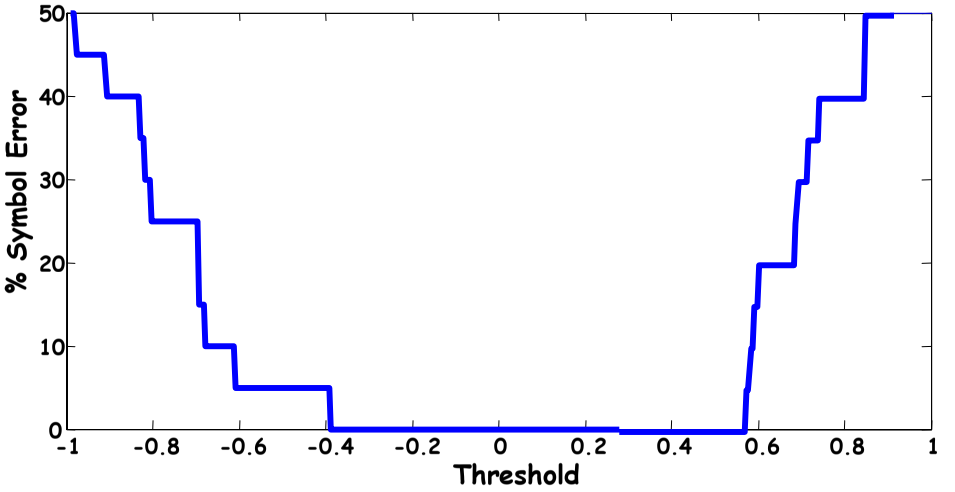
% Symbol Error
50
40
30
20
10
0
-1
-0.8
-0.6
-0.4
-0.2
0
0.2
0.4
0.6
0.8
1
Threshold

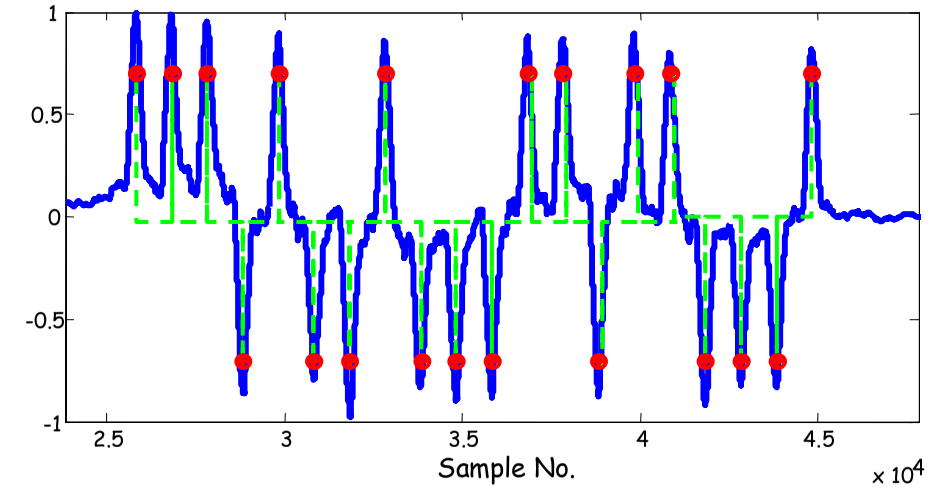
1
0.5
0
-0.5
-1
2.5
3
3.5
4
4.5
Sample No.
x 10^4

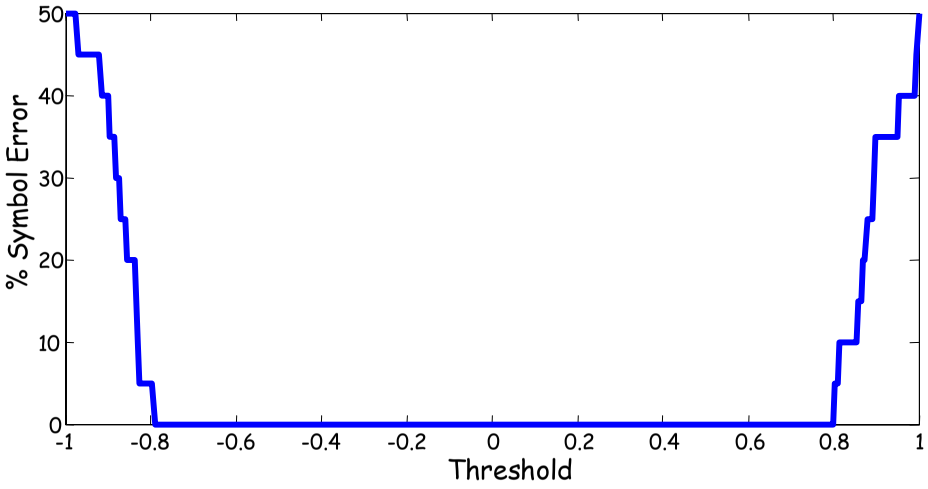
50
40
30
20
10
0
% Symbol Error
-1
-0.8
-0.6
-0.4
-0.2
0
0.2
0.4
0.6
0.8
1
Threshold

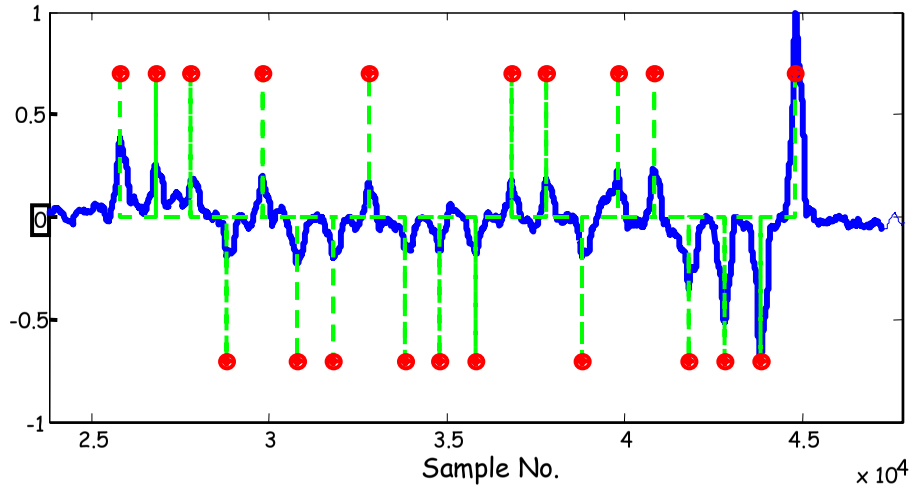
1
0.5
0
-0.5
-1
2.5
3
3.5
4
4.5
Sample No.
x 10^4

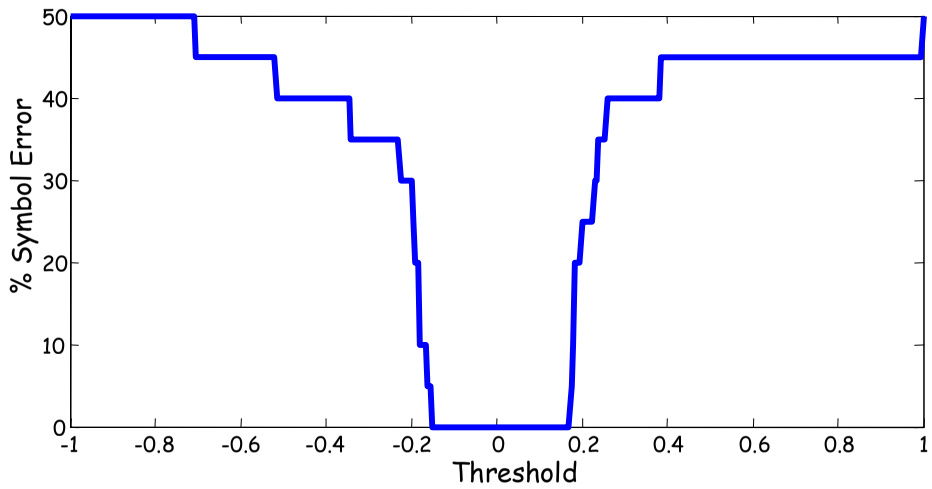
50
40
30
20
10
0
% Symbol Error
-1
-0.8
-0.6
-0.4
-0.2
0
0.2
0.4
0.6
0.8
1
Threshold

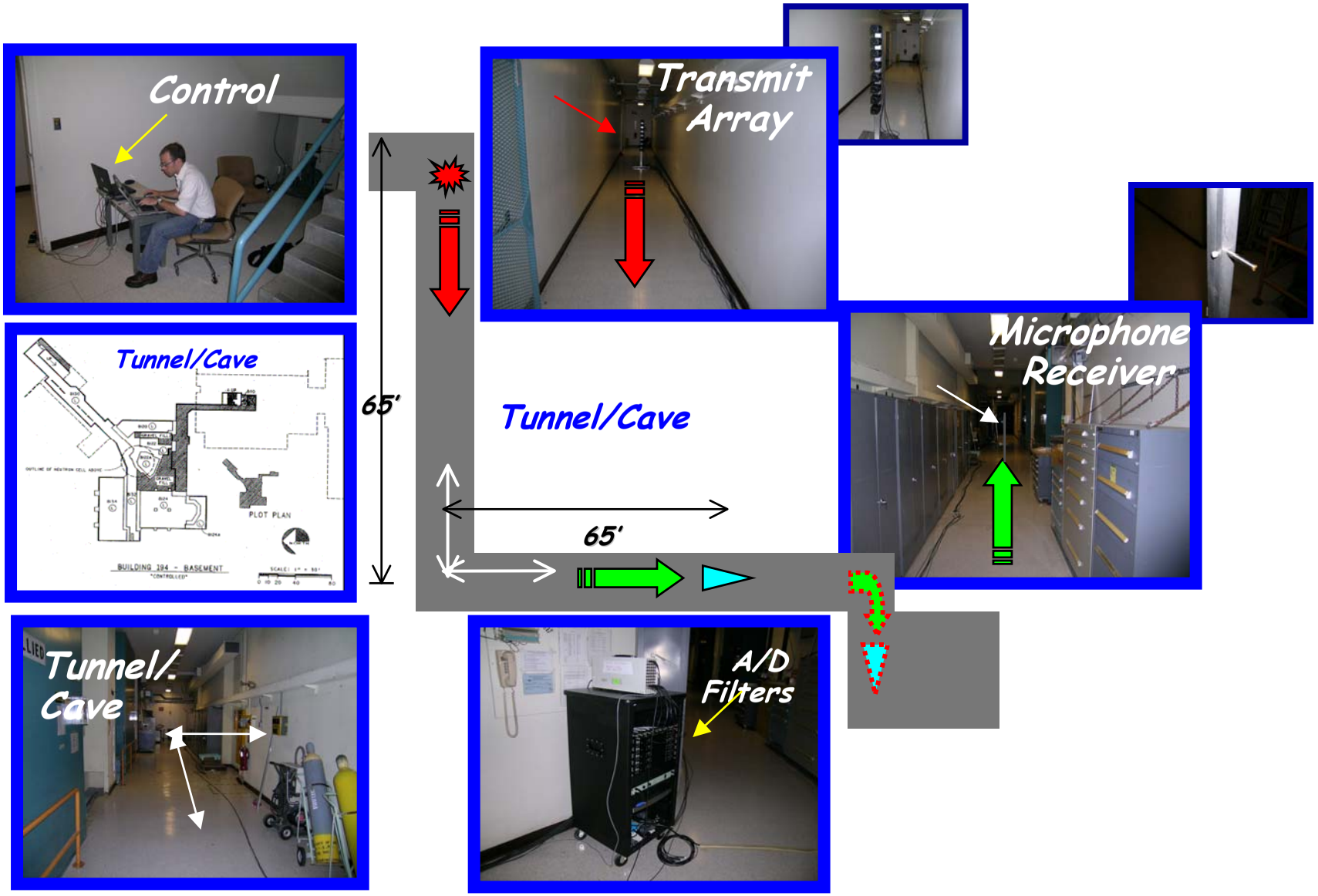
Control
Transmit Array
Microphone Receiver
Tunnel/Cave
PLOT PLAN
BUILDING 194 - BASEMENT
65'
Tunnel/Cave
65'
Tunnel/ Cave
A/D Filters

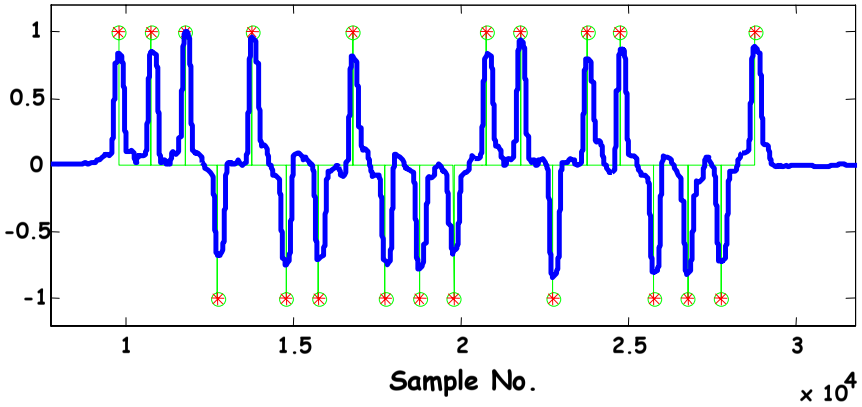
1
0.5
0
-0.5
-1
1
1.5
2
2.5
3
Sample No.
x 10^4

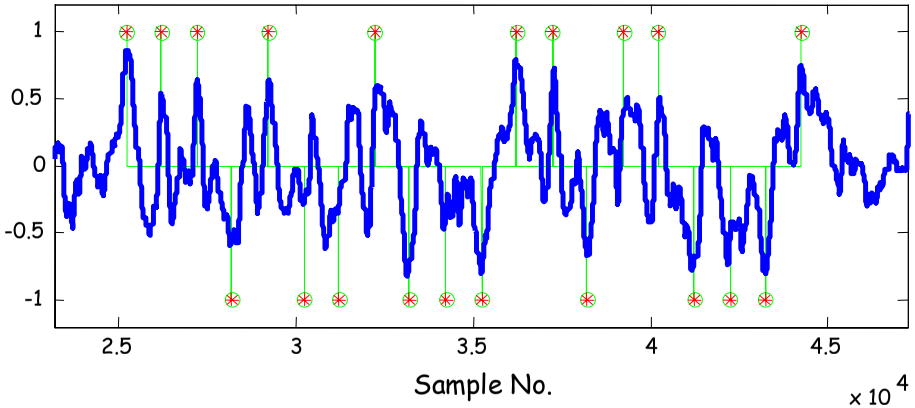
1
0.5
0
-0.5
-1
2.5
3
3.5
4
4.5
Sample No.
x 10^4

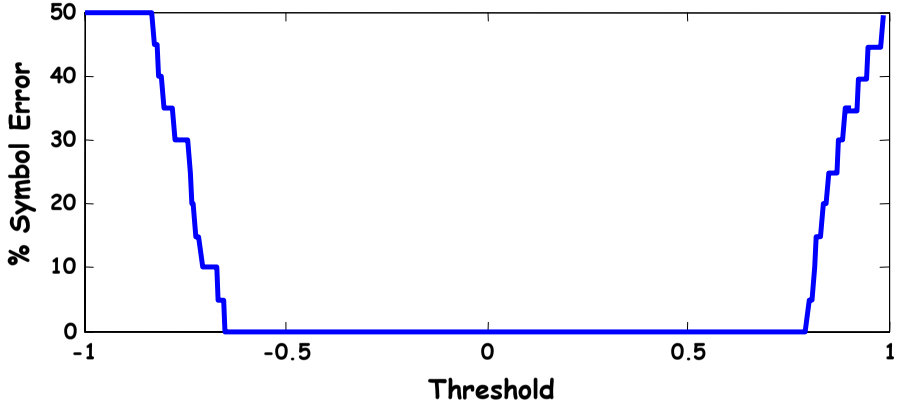
% Symbol Error
50
40
30
20
10
0
-1
-0.5
0
0.5
1
Threshold

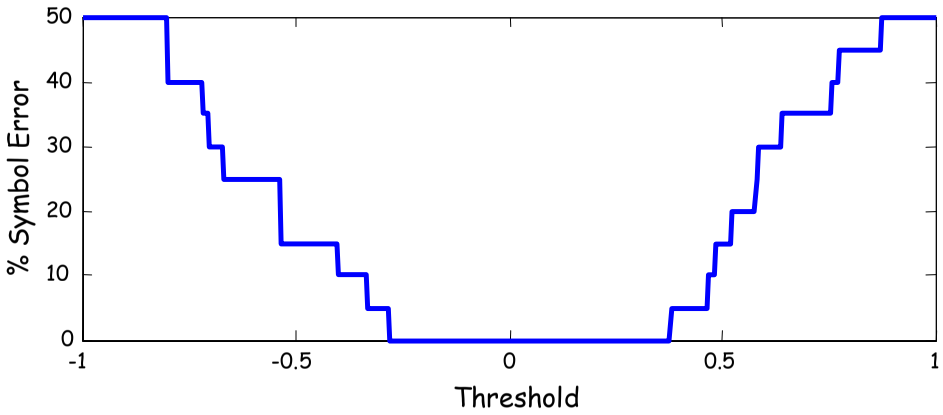
% Symbol Error
50
40
30
20
10
0
-1
-0.5
0
0.5
1
Threshold

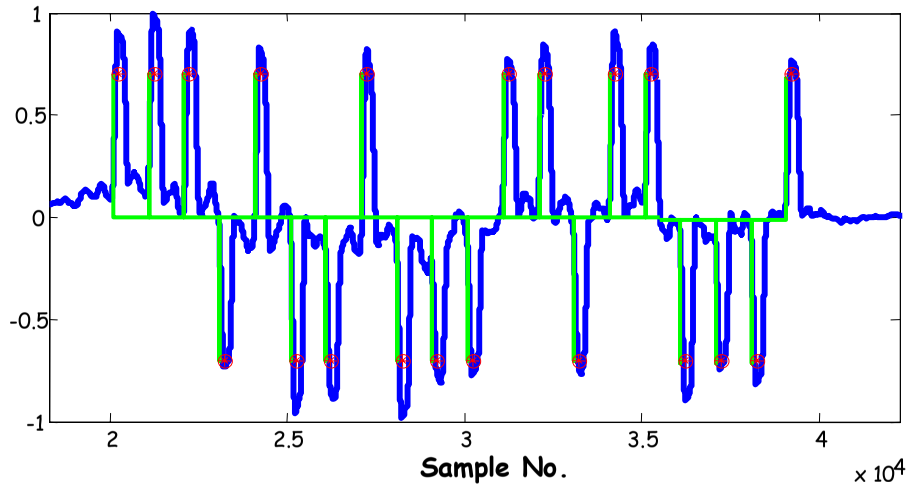
1
0.5
0
-0.5
-1
2
2.5
3
3.5
4
Sample No.
x 10^4

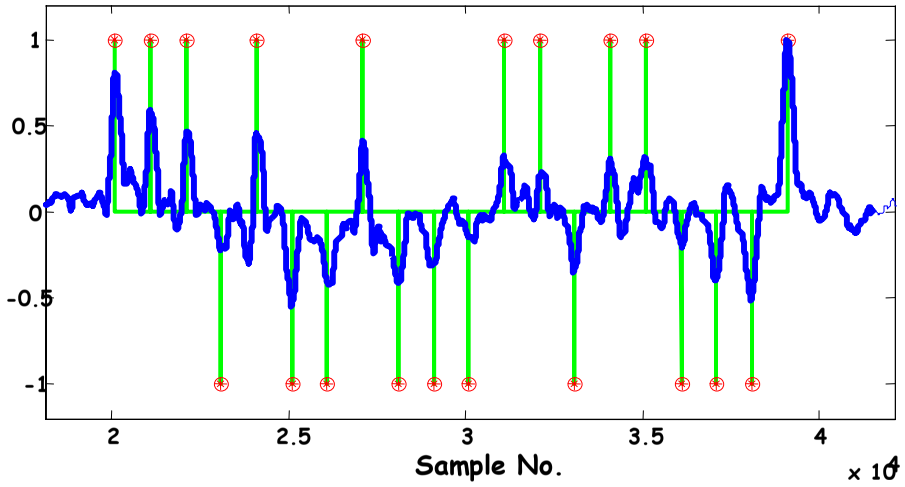
1
0.5
0
-0.5
-1
2
2.5
3
3.5
4
Sample No.
x 10^4

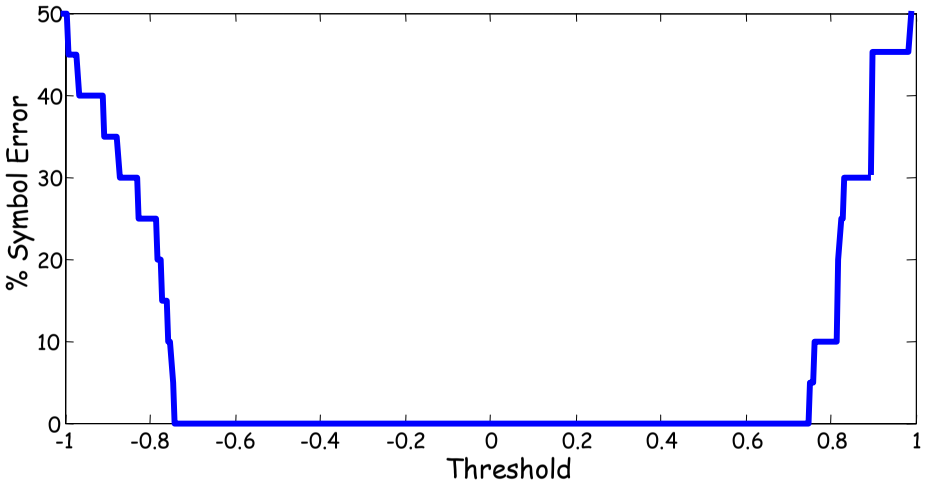
% Symbol Error
50
40
30
20
10
0
-1
-0.8
-0.6
-0.4
-0.2
0
0.2
0.4
0.6
0.8
1
Threshold

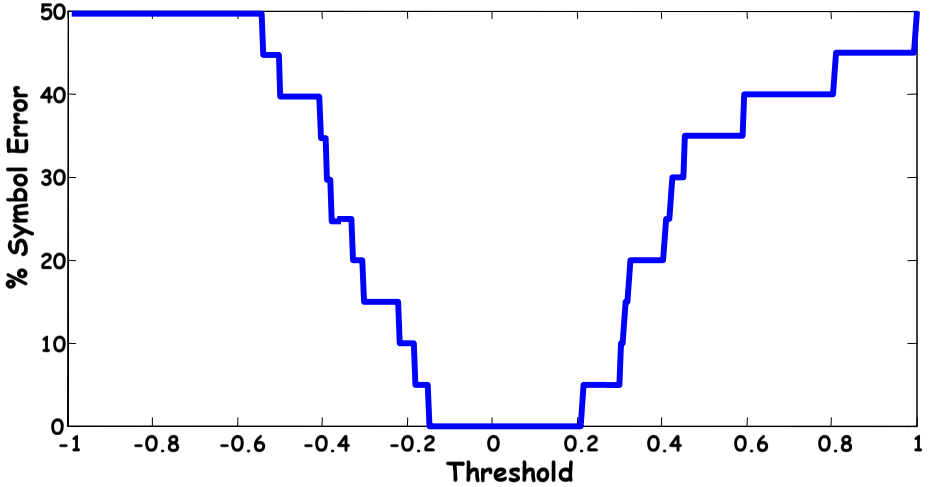
% Symbol Error
50
40
30
20
10
0
-1
-0.8
-0.6
-0.4
-0.2
0
0.2
0.4
0.6
0.8
1
Threshold

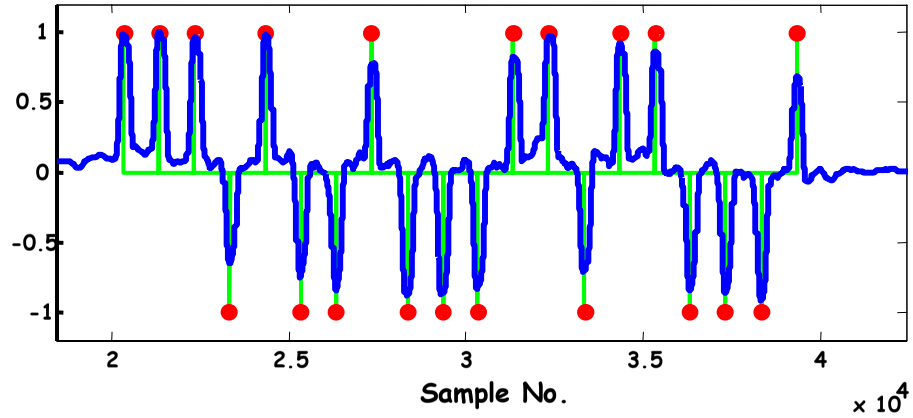
1
0.5
0
-0.5
-1
2
2.5
3
3.5
4
Sample No.
x 10^4

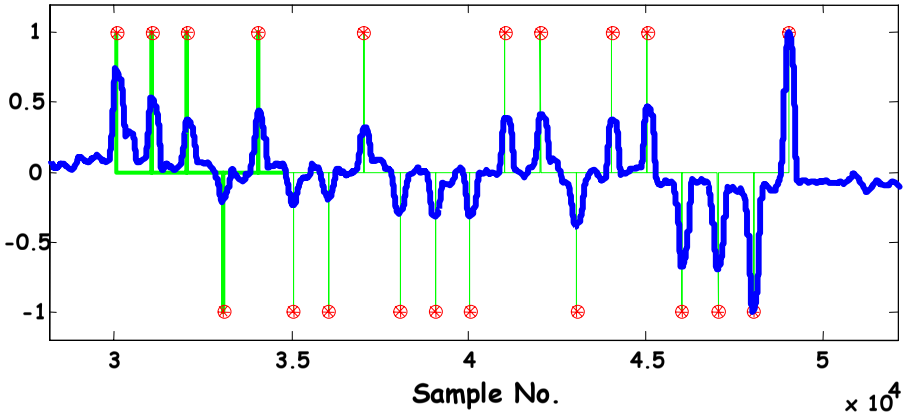
1
0.5
0
-0.5
-1
3
3.5
4
4.5
5
Sample No.
x 10^4

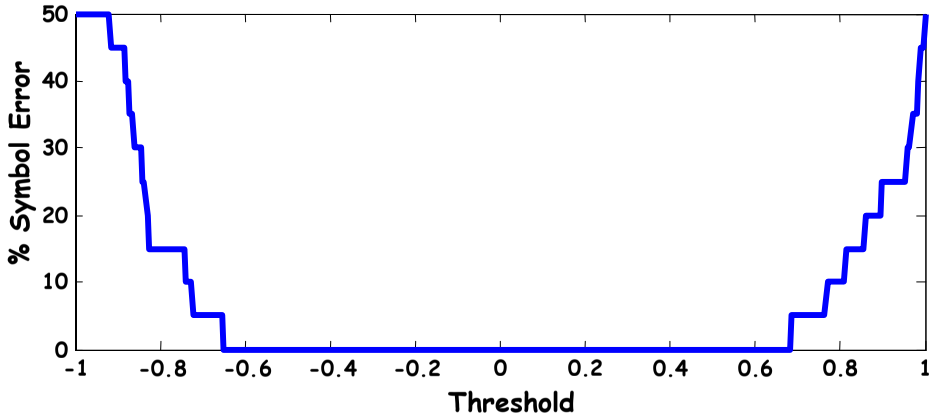
% Symbol Error
50
40
30
20
10
0
-1
-0.8
-0.6
-0.4
-0.2
0
0.2
0.4
0.6
0.8
1
Threshold

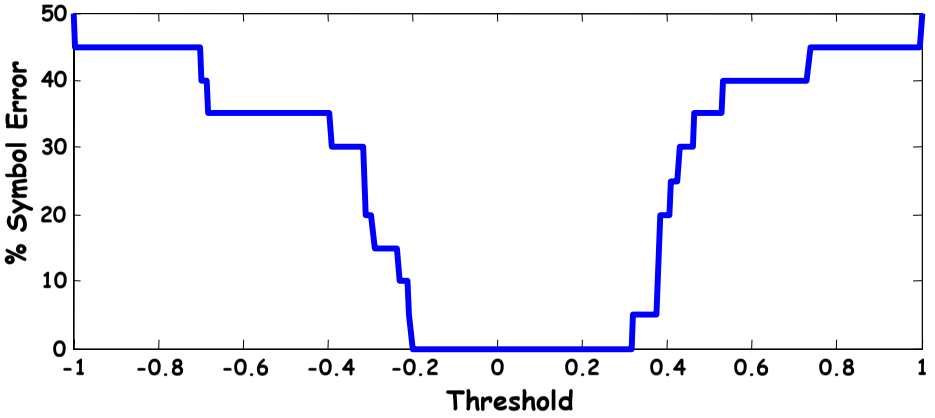
% Symbol Error
50
40
30
20
10
0
-1
-0.8
-0.6
-0.4
-0.2
0
0.2
0.4
0.6
0.8
1
Threshold

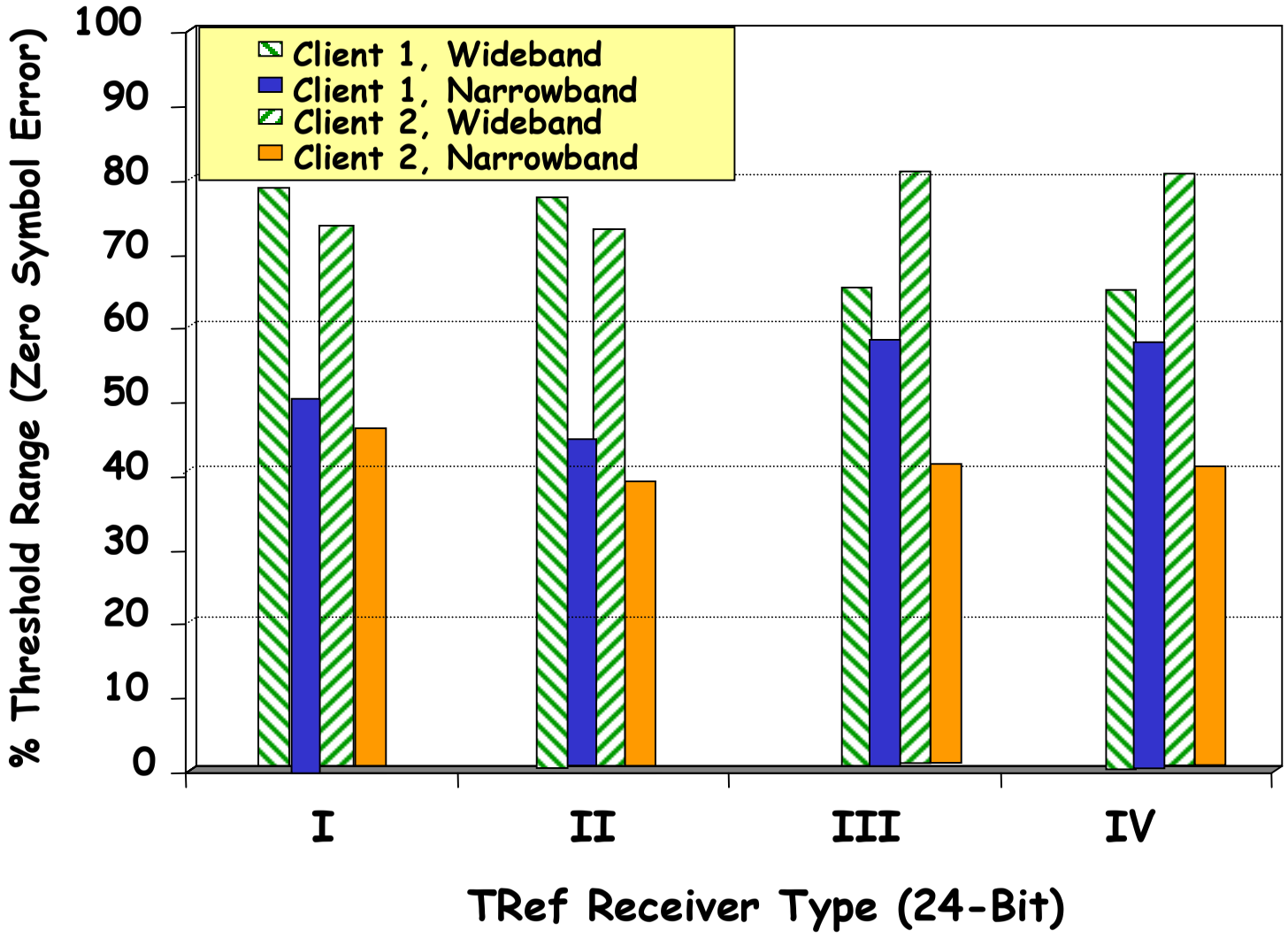
Client 1, Wideband
Client 1, Narrowband
Client 2, Wideband
Client 2, Narrowband
% Threshold Range (Zero Symbol Error)
100
90
80
70
60
50
40
30
20
10
0
I
II
III
IV
TRef Receiver Type (24-Bit)

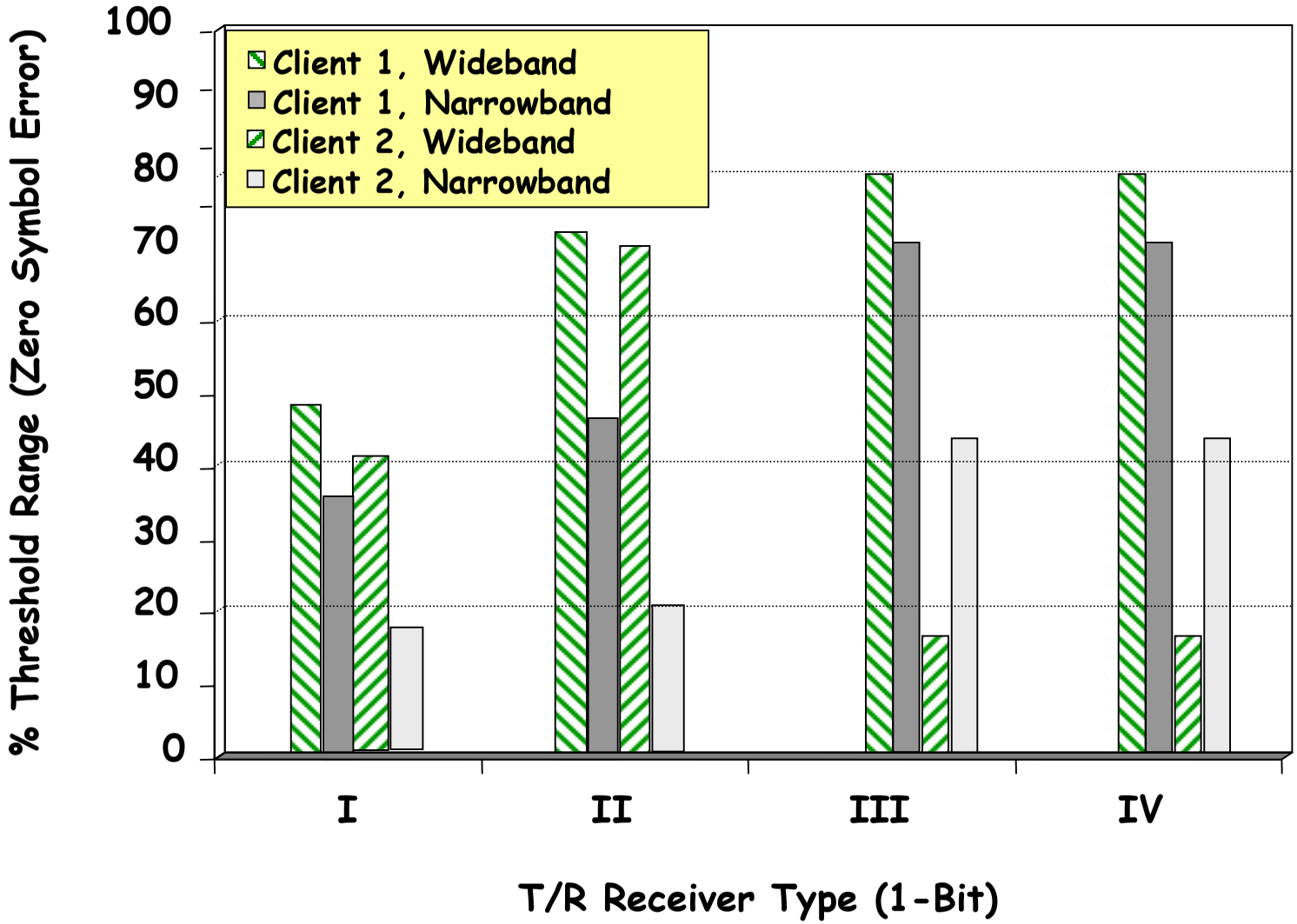
Client 1, Wideband
Client 1, Narrowband
Client 2, Wideband
Client 2, Narrowband
% Threshold Range (Zero Symbol Error)
100
90
80
70
60
50
40
30
20
10
0
I
II
III
IV
T/R Receiver Type (1-Bit)

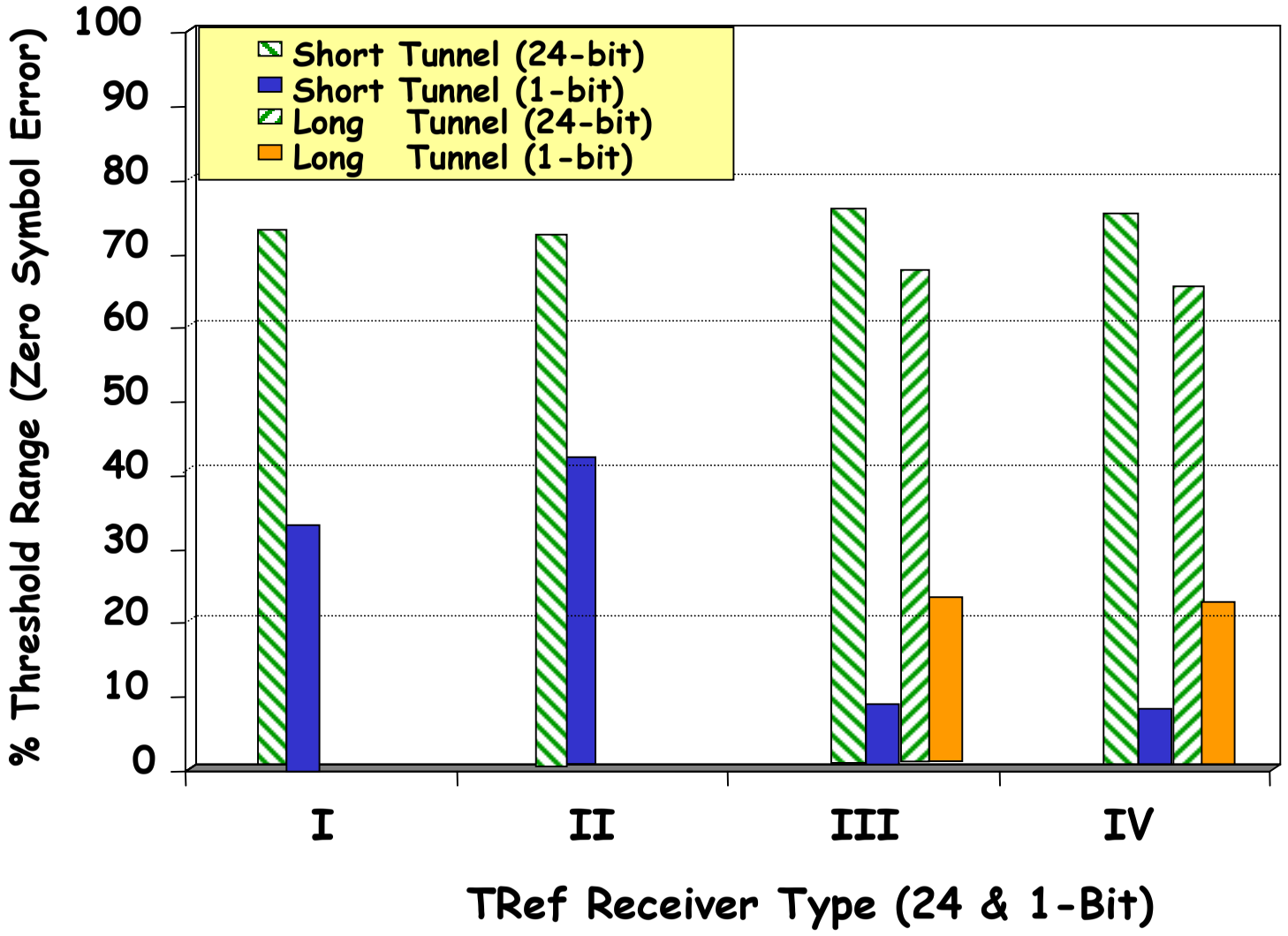
Short Tunnel (24-bit)
Short Tunnel (1-bit)
Long Tunnel (24-bit)
Long Tunnel (1-bit)
% Threshold Range (Zero Symbol Error)
100
90
80
70
60
50
40
30
20
10
0
I
II
III
IV
TRef Receiver Type (24 & 1-Bit)